Ether phospholipids modulate somatosensory responses by tuning multiple receptor functions in *Drosophila*

Takuto Suito[1,2*], Kohjiro Nagao[3], Xiangmei Deng[1,2,4], Christian Ganser[2], Takayuki Uchihashi[2,5], Motosuke Tsutsumi[2,6], Tomomi Nemoto[2,4,6], Yuji Hara[7], Makoto Tominaga[1,2,4], Takaaki Sokabe[1,2,4*]

[1] *Division of Cell Signaling, National Institute for Physiological Sciences, National Institutes of Natural Sciences, Okazaki, Japan.*

[2] *Exploratory Research Center on Life and Living Systems, National Institutes of Natural Sciences, Okazaki, Japan.*

[3] *Department of Biophysical Chemistry, Kyoto Pharmaceutical University, Kyoto, Japan.*

[4] *Graduate Institute for Advanced Studies, SOKENDAI, Hayama, Japan*

[5] *Department of Physics, Nagoya University, Nagoya, Japan*

[6] *Division of Biophotonics, National Institute for Physiological Sciences, National Institutes of Natural Sciences, Okazaki, Japan.*

[7] *School of Pharmaceutical Sciences, University of Shizuoka, Shizuoka, Japan*

*To whom correspondence should be addressed: 5-1 Higashiyama, Okazaki, Aichi 444-8787, Japan, Tel.: 81-564-59-5287; E-mail: suito@nips.ac.jp, sokabe@nips.ac.jp

ABSTRACT

Transient receptor potential (TRP) and PIEZO channels are known receptors for physical stimuli such as temperature and mechanical touch in sensory nerves. Since these receptors are localized in the plasma membrane, the regulation of sensory receptor activity by plasma membrane lipids has recently attracted attention. In this study, we focused on ether phospholipids (ePLs), which are abundant in neurons, and analyzed their role in somatosensation using *Drosophila* as a model. Reduced warmth avoidance was observed with ePL synthesizing gene knockout or knockdown in warmth-sensitive TRPA1-expressing neurons. The temperature threshold for *Drosophila* TRPA1 channels significantly decreased in presence of ePLs. In addition, we found that ePLs modulate the mechanosensory behavior and activation properties of the mechanosensitive channel PIEZO. Finally, we revealed that ePLs affect physicochemical properties of the plasma membrane, such as membrane tension and lipid order, in culture cells. Our study identified ePLs as crucial regulators of multiple somatosensation modalities in *Drosophila*. Effects due to alteration of cellular membrane properties and activity modulation of sensory receptors.

INTRODUCTION

The sensory system is indispensable to detect environmental parameters. Sensory perception is initiated by the activation of sensory receptors in sensory nerves and other type of cells, which convert external stimuli into electrical or chemical signals. Transient receptor potential (TRP) channels[1, 2, 3] and PIEZO channels[4] are considered receptors for physical stimuli such as temperature and mechanical touch, and their roles in sensory processing and the underlying mechanisms[5, 6] have been extensively studied[7].

As these receptors are membrane proteins, the functional interaction between ion channels and membrane lipids has been key for resolving their activation mechanisms and cellular functions[8]. The activity of many TRP channels is regulated by a wide variety of lipid molecules, such as phosphatidylinositol phosphates, fatty acids (FA) and their metabolites, endocannabinoids, lysophospholipids, and sphingolipids[9, 10, 11, 12]. The modes of action of these lipids are either direct or indirect, modulating TRP channel activity positively or negatively depending on cellular context and signaling pathways. Similarly, PIEZO channel activities are modulated by lipids. The activity of PIEZO1 is affected by the enrichment of either saturated or polyunsaturated FA (PUFAs) in membrane phospholipids[13, 14]. Phosphatidylserine (PS) may interact with PIEZO1, and the asymmetric distribution of PS in the lipid bilayer is critical for the channel activity[15]. These tight functional linkages between sensory ion channels and lipid molecules exemplify their importance in cellular functions.

A limited number of studies evaluated the physiological significance of lipid molecules on sensory responses in animals. For example, PUFA-containing phospholipids are highly enriched and play a significant role in the brain[16, 17]. In *C. elegans*, arachidonic acid-containing phospholipids modulate the function of touch receptor neurons[18]. In *Drosophila*, an increase in the content of linoleic acid in sensory neurons changes TRPA1 activity and the preferred temperature of larvae[19]. Recently, it has been reported that linoleic acid increases PIEZO2 activity, and that linoleic acid supplementation improves Angelman Syndrome-associated mechanosensory deficits in mice[14]. These results suggest that lipid molecules may modulate the responsiveness and sensitivity of ion channels, thereby influencing neural function and the consequent physiological outputs.

An interesting lipid species in neural tissues is an ether phospholipid (ePL) identified in cancer cells in the 1960s[20]. ePLs constitute 20% of the lipid content in the mouse central

70 nervous system (CNS) appearing as plasmalogen-type phosphatidylethanolamine (PE), which
71 harbors a vinyl–ether bond at the *sn*-1 position of the glycerol backbone[21]. ePLs are synthesized
72 from dihydroxyacetone phosphate in the peroxisome and transported to the endoplasmic
73 reticulum for further processing. Deficiency in synthesis enzymes of ePLs such as
74 alkylglycerone phosphate synthase (AGPS) can cause rhizomelic chondrodysplasia punctata[22], a
75 peroxisomal disorder resulting in diverse developmental dysfunctions, including neuronal
76 disorders[23]. In addition, ePLs have been implicated in neurodegenerative diseases; lower
77 plasmalogen ePL content has been reported in Alzheimer's disease, Parkinson's disease,
78 Huntington's disease, etc[23]. Although the causal relationship between disease progression and
79 the reduction of ePLs has not been clarified, ePLs may be a functionally important component in
80 the CNS. In the peripheral nervous system, conversely, there is so far no evidence as to the
81 existence and function of ePLs.
82 Here, we combined lipidomic, behavioral, electrophysiological analyses, and
83 measurements of the physicochemical properties of cell membranes to demonstrate the
84 functional linkage between ePLs and sensory functions in *Drosophila*. Lipid analysis revealed
85 the existence of ePLs, particularly ether phosphatidylethanolamines (ePEs), in neural tissues.
86 Then, we analyzed thermoregulatory behaviors in larvae and found that an *AGPS* knockout or
87 knockdown in warm-sensitive, TRPA1-expressing neurons decreased warmth avoidance.
88 Electrophysiological analyses of TRPA1 revealed the effect of ePLs on lowering the temperature
89 threshold for TRPA1 activation. In addition, we found that *AGPS* knockout or knockdown in
90 mechanosensitive, PIEZO-expressing neurons decreased mechanical nociception. This was
91 caused by a decreased mechano–sensitivity of PIEZO in the absence of ePLs, since we observed
92 enhanced PIEZO activation by ePLs *in vitro*. Finally, we analyzed the effects of ePLs on the
93 physicochemical properties of cell membranes and found that ePLs altered membrane tension
94 and lipid order. Our work demonstrates that ePLs play pivotal roles in optimizing multiple
95 somatosensory modalities by altering cell membrane properties and tuning functions of distinct
96 receptors.

RESULTS

Ether phospholipids are enriched in Drosophila neurons

Given the limited number of studies reporting ePLs synthesis in *Drosophila melanogaster*, we first confirmed the presence of ePLs in different tissues. We dissected various tissues from third instar larvae or used the whole body to quantify mRNA expression level of *AGPS*, an essential enzyme for ePL biosynthesis[24] (Fig. 1a). *AGPS* was abundantly expressed in the CNS (4.5 times more than in whole body), whereas trace levels of expression were observed in the fat body and carcass (Fig. 1a). *AGPS* expression was also analyzed in peripheral sensory neurons in the body wall. Using magnetic-bead-based cell sorting, we isolated *ppk*-positive sensory neurons, a subset of polymodal, class IV multidendrtic neurons[25]. The *AGPS* expression level in the magnetic bead-bound (class IV neuron enriched) fraction was significantly higher than in the bead unbound (other cells from the body wall) fraction ($p < 0.01$ in Student's t-test, Fig. 1b). These findings suggest that ePL plays functional roles in central and peripheral neurons in *Drosophila*.

Next, to determine ePL composition in *Drosophila* membrane phospholipids, we performed a comprehensive lipid analysis of phospholipid species, including ePLs, in the whole body and the CNS. Specifically, two major classes of phospholipids in *Drosophila*[26], PE and phosphatidylcholine (PC), were analyzed (Fig. 1c–e, Supplementary Fig. 1a, b, Supplementary Table 1–4). The proportion of ePEs in total PEs was 0.64% ± 0.08% in the whole body and 16.6% ± 1.5% in the CNS (Fig. 1c, d). In contrast, only trace level of ether PCs (ePCs) were observed in the PC for both the whole body and the CNS (Fig. 1e and Supplementary Table 2, 4).

Next, we established *AGPS* knockouts (*AGPS* KO) using CRISPR-Cas9 to confirm the functional roles of AGPS in ePL synthesis (Supplementary Fig. 1c). Homozygous *AGPS* KO flies ($AGPS^{KO}$) expressed a negligible level of *AGPS* mRNA (Supplementary Fig. 1d), without obvious growth defects such as a delay in pupariation timing (Supplementary Fig. 1e). The lipid analysis clearly demonstrated complete depletion of ePL molecules in both the whole body and the CNS of $AGPS^{KO}$ (Fig. 1c–e, Supplementary Fig. 1a, b, Supplementary Table 1–4), emphasizing the essential role of *AGPS* in ePL synthesis in *Drosophila*. *AGPS* heterozygous KO flies ($AGPS^{KO/+}$) showed a significant reduction in *AGPS* expression level ($p < 0.001$ in Student's t-test, Supplementary Fig. 1d) but no changes in the total amount of ePLs compared to control (Fig. 1c, Supplementary Fig. 1a, b, Supplementary Table 1, 2).

In mammals, the major ePL molecule is of the plasmalogen type, in which an *sn*-1 acyl chain is attached to the glycerol backbone via a vinyl–ether bond. To identify the *sn*-1 and *sn*-2 acyl chain profiles of ePEs in *Drosophila*, we performed product ion scan analysis for major ePEs including ePE (34:1), ePE (36:1), ePE (36:2), and ePE (36:3) in the CNS sample (Supplementary Fig. 2a–j). ePE (36:2) appeared to be the most abundant among all ePEs in *Drosophila*'s CNS (Fig. 1d). The major product ion of ePE (36:2) coincided with linoleic acid (C18:2) (Supplementary Fig. 2h), indicating that the *sn*-2 ester-bound acyl group is C18:2, and the ether-linked *sn*-1 hydrocarbon chain was octadecyl alcohol without double bonds (O-18:0). The other analyzed ePEs harbored either palmitoleic acid (C16:1), oleic acid (C18:1), or linolenic acid (C18:3) at the ester-linked acyl chain, and O-18:0 at the ether-linked acyl chain (Supplementary Fig. 2b, e, j). These data suggested that ePLs, especially ePEs, are abundantly present in *Drosophila* neurons. Moreover, ePEs in *Drosophila* neurons appear to contain an ether bond, but not a vinyl–ether bond, at the *sn-1* position, in contrast to the most common ePL molecule found in mammals.

AGPS mutation alters thermoregulatory behaviors in Drosophila

A previous study reported that alterations in membrane lipid composition can affect temperature preference in *Drosophila*[19]. Since ePLs may modulate the physicochemical properties of the plasma membrane, we hypothesized that ePL synthesis should affect sensory responses, particularly to physical stimuli. Therefore, we first investigated the effect of ePLs on thermosensation in larvae. We subjected late third instar larvae (120 hr after egg laying, AEL) to a temperature gradient assay (8ºC–35ºC) to examine their thermotactic behavior. Control (w^{1118}) and heterozygous $AGPS^{KO/+}$ larvae distributed through the temperature gradient with peaks around 20ºC, avoiding lower and higher temperatures (Fig. 2a). However, two independent clones of *AGPS* homozygous KO ($AGPS^{KO1/KO1}$ and $AGPS^{KO2/KO2}$) lost a clear peak in their distribution, showing increased fractions in high temperature zones than the control and $AGPS^{KO/+}$ larvae (Fig. 2a). Specifically, the proportion of larvae distributed over 25ºC zones was 15.5% ± 1.8% in control, whereas significant increases (>30%) were observed in $AGPS^{KO}$ clones (35.8% ± 3.8% in $AGPS^{KO1/KO1}$, 33.0% ± 4.0% in $AGPS^{KO2/KO2}$; $p < 0.001$ in Mann–Whitney U-test, Fig. 2b). These results demonstrated that ePL loss leads to an abnormal thermotactic phenotype in *Drosophila*.

158 To investigate whether sensory functions are affected by the absence of ePLs, we used
159 the GAL4-UAS system for tissue specific *AGPS* knockdown in thermosensory neurons reported
160 to express TRP channels involved in thermotactic behaviors. We used GAL4 lines labeling
161 TRPA1-positive neurons involved in warm temperature avoidance[27] and lines labeling TRPL-[28]
162 and Inactive (Iav)-positive neurons[29] involved in cool temperature avoidance. Among them,
163 *TRPA1-AB*^{GAL4}-induced *AGPS* knockdown resulted in a significant increase in the fraction of
164 larvae distributed in high temperature zones ($p < 0.001$ in Mann–Whitney U-test, Fig. 2c, d),
165 which resembled the *AGPS*^{KO} phenotype (Fig. 1a, b). Moreover, the phenotypes of *AGPS*
166 knockdown in TRPA1-A/B neurons were comparable to those in *TRPA1-A/B* KO
167 (*TRPA1-AB*^{GAL4}) flies (Fig. 2e, f). To further confirm that thermotactic behaviors depend on
168 *AGPS*, larvae were subjected to a thermal two-choice assay (20ºC and 29ºC). The higher
169 temperature was highly aversive for control larvae, whereas reduced or no avoidance was
170 observed in *AGPS*^{KO} (Fig. 2g) or *AGPS* knockdown in TRPA1-A/B neurons (Fig. 2h),
171 respectively. Overall, these results strongly suggest that *AGPS* plays a crucial role in modulating
172 the thermosensory responses of TRPA1-A/B-expressing neurons in *Drosophila*.
173 In *Drosophila melanogaster*, there are four functional TRPA1 splicing variants
174 expressed in distinct sensory neurons[30, 31] and TRPA1-A/B receptors are exclusively present in
175 cell subsets of the CNS in larvae[27]. We observed the morphology of TRPA1-A/B-expressing
176 neurons in the CNS and found no obvious structural changes with *AGPS* knock down
177 (Supplementary Fig. 3). This suggested that functional reduction of *AGPS* may not alter the
178 development and cell fate of the TRPA1-A/B neurons.
179
180 ***Ether phospholipids modulate the temperature threshold for dTRPA1 activation***
181 We hypothesized that AGPS-produced ePLs influence thermosensation in larvae by directly
182 modulating thermosensory proteins such as TRPA1. To elucidate the functional role of ePLs in
183 temperature-evoked activation of TRPA1, we conducted an electrophysiological analysis using
184 cultured cells. First, we tested dTRPA1-A isoforms expressed in mammalian HEK293T cells.
185 HEK293T cells intrinsically harbor ePLs; ePEs and ePCs accounted for 4.2% ± 0.01% of total
186 PE and 15.8% ± 0.1% of total PC, respectively (Supplementary Fig. 4a–d, Supplementary Table
187 5, 6). To deplete ePLs from cells, we generated an *AGPS* KO cell line using CRISPR-Cas9. Both
188 ePEs and ePCs were successfully depleted in the absence of functional human AGPS

189 (Supplementary Fig. 4a–d, Supplementary Table 5, 6). Next, we transiently expressed dTRPA1-A
190 in wild type and *AGPS* KO cells; there was no difference in heat-induced dTRPA1-A activation
191 (temperature threshold for activation and the current density) with presence or absence of ePLs
192 (Supplementary Fig. 4e–h). We also tested dTRPA1-A chemical responses by stimulating with an
193 electrophilic TRPA1 activator, allyl isothiocyanate (AITC). Although we observed a small
194 increase in the current density at a low AITC concentration (20 μM) in *AGPS* KO cells, such
195 difference was not observed at a saturated concentration (300 μM) (Supplementary Fig. 4i, j).

196 Since HEK293T cells were enriched in ePCs rather than ePEs, the major endogenous
197 ePLs in *Drosophila* CNS, we used S2R+ cells, a *Drosophila* embryonic cultured cell line, as they
198 lack the ability to synthesize ePLs. Accordingly, we established ePL-producing S2R+ cell lines
199 using two distinct approaches: (i) supplementation of alkylglycerol (AG) as a precursor of ePLs
200 to wild type cells to bypass the requirement of AGPS, or (ii) supplementation of fatty alcohol to
201 cells overexpressing dAGPS to drive ePL biosynthesis (Fig. 3a). The lipid analysis revealed
202 successful ePL production in S2R+ cells with both approaches (Fig. 3b–e, Supplementary Table
203 7, 8). Importantly, the production of ePEs, but not ePCs, was primarily induced, consistent with
204 the ePL composition in larvae (Fig. 1d, e). A product ion scan analysis demonstrated that
205 supplementation with hexadecanoyl glycerol (16-AG) induced the production of ePE (32:1) and
206 ePE (34:1), considered to introduce palmitoleic acid (C16:1) and oleic acid (C18:1) at the
207 ester-linked position, respectively (Supplementary Fig. 5a, b), suggesting that a hexadecyl
208 alcohol without double bonds (O-16:0) was bound at ether-linked position. Supplementation with
209 octadecyl alcohol (18-OH) to AGPS-expressing cells resulted in the production of ePE (34:1)
210 and ePE (36:1) containing octadecyl alcohol (O-18:0) at ether-linked positions (Supplementary
211 Fig. 5c). Thus, the composition of the *sn*-1 hydrocarbon chain in ePLs appears to reflect the
212 features of the supplemented AG or fatty alcohol.

213 First, we evaluated the temperature-dependent dTRPA1-A activation using S2R+ cells
214 supplemented with 16-AG or octadecanoyl glycerol (18-AG) (Fig. 4). The average temperature
215 threshold for dTRPA1-A activation was 22.1ºC ± 0.4ºC in control S2R+ cells (Fig. 4a, d),
216 becoming significantly decreased ($p < 0.05$ in Dunnett test,) to 20.8ºC ± 0.3ºC when S2R+ cells
217 were supplemented with 18-AG (Fig. 4c, d). Although not significant ($p = 0.06$), 16-AG
218 supplementation to S2R+ cells resulted in decreasing tendency for the temperature threshold to
219 21.1ºC ± 0.3ºC (Fig. 4b, d). However, we did not observe alterations in maximum current

220 densities due to heat or AITC stimulation in ePL-producing cells (Fig. 4e–g). Consistent with the
221 18-AG supplementation, 18-OH supplementation to AGPS-expressing S2R+ cells significant
222 decreased the temperature threshold for dTRPA1-A activation compared to control cells (20.3ºC
223 ± 0.7ºC vs. 24.0ºC ± 1.2ºC; $p < 0.05$ in Student's t-test, Supplementary Fig. 6a–c). Likewise,
224 neither heat- nor AITC-evoked current densities were affected (Supplementary Fig. 6d–f).
225 dTRPA1-B properties were also tested in ePL-producing S2R+ cells. Both the temperature
226 threshold for activation and the maximum heat-evoked current densities were not altered in
227 presence of ePLs (Supplementary Fig. 7a–d). In contrast, AITC-induced current density was
228 significantly reduced in ePL-producing S2R+ cells both at low (30 μM) and high concentrations
229 (300 μM) ($p < 0.05$ in Student's t-test, Supplementary Fig. 7e, f). Taken together, these results
230 suggest that ePLs, particularly ePEs in the plasma membrane, reduce the temperature threshold
231 for heat-evoked dTRPA1-A activation, which may be important for thermosensory function in
232 animals.
233
234 ***Mechanosensory function is regulated by ether phospholipids***
235 Difference in membrane lipid composition reportedly leads to alterations in membrane properties
236 thereby affecting the activity of mechanosensory channels[13, 14]. This evidence together with our
237 findings led us to expect that mechanosensory function could also be affected by *AGPS* mutation
238 and associated ePL loss in *Drosophila*. To investigate this point, we evaluated larval
239 mechanosensory responses. First, we assessed tactile sensation by measuring responses to a
240 gentle touch to the nose of freely moving larva; no difference in responses was observed between
241 control and $AGPS^{KO}$ larvae (Fig. 5a). Second, we characterized mechanical nociception by
242 poking a larva using von Frey filaments of three different forces (20.1, 47.0, and 70.0 mN).
243 Nociceptive rolling behavior to the weakest force (20.1 mN), but not stronger ones, was
244 significantly decreased in $AGPS^{KO}$ compared to control larvae ($p < 0.05$ in Student's t-test, Fig.
245 5b). We then used different GAL4 lines for *AGPS* knockdown to identify the mechanosensory
246 neurons involved in the reduction in mechanical nociception. Several receptor genes have been
247 reported as responsible for the von Frey filament responses, including *PIEZO*[32], *TRPA1-C/D*[30, 33],
248 *ppk*[34], and *painless*[35]. When *AGPS* RNAi was induced using *PIEZO-GAL4* and $TRPA1\text{-}CD^{GAL4}$, a
249 significant decrease in the response to the von Frey filament (20.1 mN) was observed ($p < 0.05$

250 in Dunnett test) (Fig. 5c). These results suggest that AGPS and its product ePL could modulate
251 responsiveness in mechanosensory neurons.
252 This result drove us to investigate whether ePLs modulate the activation of a PIEZO
253 mechanosensor. The PIEZO response to its activator Yoda1[36] was evaluated through Ca^{2+}
254 imaging to test the functional role of ePLs in channel activation. PIEZO-expressing S2R+ cells
255 were stimulated with Yoda1 perfusion, which evoked a stochastic Ca^{2+} increase in a small
256 number of cells (11.1% ± 3.1%; Fig. 6a, b, d, and e). When S2R+ cells were supplemented with
257 18-AG before the experiments, Yoda1 perfusion elicited significantly higher Ca^{2+} increases in a
258 larger cell population (28.7% ± 3.8%, $p < 0.01$ in Student's t-test; Fig. 6 a, c–e). These results
259 suggested that ePLs enhance PIEZO mechanosensitivity, thereby regulating animals' mechanical
260 responses. Altogether, our findings demonstrated that loss of *AGPS* and ePLs influence both
261 thermosensory and mechanosensory functions in *Drosophila*, and that ePLs play crucial roles in
262 modulating the activity of multiple sensory ion channels.
263
264 ***Ether phospholipids alter membrane tension and lipid order***
265 Previous reports have shown that lipid modulation alters membrane tension, which can impact
266 the activity of sensory channels[13, 37]. To get further insights into the effects of ePEs on membrane
267 properties in S2R+ cells, we used different approaches to quantify membrane tension and lipid
268 order.
269 First, we measured membrane tension through atomic force microscopy (AFM) force
270 curve measurement. Parts of the cell surfaces were scanned with AFM while intermittently
271 recording force curves to determine the Young's modulus, which reflects membrane tension at
272 each point (Supplementary Fig. 8a). The median value of the calculated Young's modulus in
273 control was 0.95×10^5 Pa (Fig. 7a) while that in 18-AG supplemented S2R+ cells was 2.4×10^5
274 Pa, significantly higher ($p < 0.001$, Mann–Whitney U-test) than control cells. Second, we utilized
275 a Flipper-TR probe to measure membrane tension. When the probe is incorporated into the
276 plasma membrane, the emitted fluorescent lifetime correlates with the membrane tension[38]. A
277 longer fluorescent lifetime was observed for 18-AG supplemented S2R+ cells compared to the
278 control (Fig. 7b, Supplementary Fig. 8b). These distinct measurements consistently showed an
279 increase in membrane tension in the presence of ePLs in the plasma membrane.

280 Last, we assessed the lipid order using a LipiORDER Dye[39]. A significant red shift ($p <$
281 0.001, Mann–Whitney U-test) in fluorescence spectrum was observed in 18-AG supplemented
282 S2R+ cells (Fig. 7c–e), suggesting that ePE-harboring membranes are in more lipid-disordered
283 states than ePE-depleted membranes. Taken together, these results demonstrate that ePEs modify
284 the physicochemical properties of the plasma membrane, which potentially leads to changes in
285 the activity and/or sensitivity of sensory proteins, such as TRPA1 and PIEZO. Further, the
286 membrane properties of ePL-containing neurons may be altered as well, which could contribute
287 to proper sensory tuning in *Drosophila*.

288 **DISCUSSION**

289 In this study, we discovered a unique lipid molecule, ePLs, in neurons regulating sensory
290 functions in *Drosophila.* ePLs have received increased attention due to their functional
291 association with neurodegenerative diseases and metabolic disorders accompanied by systemic
292 inflammation; potential roles such as being a scavenger of oxidative stress and a reservoir of
293 fatty acid second messengers[40], which could modulate the function of ion channels[41], have been
294 proposed. Recent studies have explored their involvement in ferroptosis and cancer treatment[42].
295 Even when ePLs are closely linked to many physiological and pathological events, the
296 underlying mechanisms and specific targets of ePLs remain unclear. Our data demonstrate that
297 ePLs are required for intrinsic sensory responses by modulating the responses of multiple
298 sensory proteins, such as TRPA1 and PIEZO. The regulatory roles of ePLs on ion channel
299 activity are open for discussion as there is a small number of studies available. Presence of
300 PUFAs in the *sn*-2 position of glycerol backbone in ePLs and their metabolites has been
301 discussed as direct activators of ion channels[40]. Also, he ion transport activity of sarcosomal
302 sodium–calcium exchanger was reported to be enhances in plasmalogen-containing
303 proteoliposome [43]. However, there is few evidence that ePLs can modulate channel activity.

304 The functional correlation between ePLs and ion channels might be, at least partially,
305 explained by the alteration of membrane properties. Previous research on mouse PIEZO1
306 showed that an increase in saturated FA in the cell membrane negatively regulates channel
307 activity by bringing the membrane to an "ordered" state[13]. Since our LipiORDER analysis
308 revealed that the membrane in ePL-lacking control S2R+ cells exhibited a much more "ordered"
309 state than ePL-producing cells (Fig. 7e), the lower activity of *Drosophila* PIEZO1 in control cells
310 could result in a more ordered state of the cell membrane in the absence of ePLs. In addition, our
311 AFM and Flipper-TR imaging-based assays demonstrated that ePLs increase cell membrane
312 tension (Fig. 7a, b). Since PIEZO1 responds to changes in cell membrane tension and
313 deformation[44], the increased activity observed in ePL-producing S2R+ cells may be due to
314 altered force thresholds for inducing cell membrane deformation. Regarding TRPA1, it remains
315 unclear how the physicochemical properties of the cell membrane influence the temperature
316 sensitivity of TRPA1 and other thermosensitive TRP channels. Previous research has shown that
317 eicosapentaenoic acid and its derivatives modulate mammalian thermosensitive TRPV4
318 responses to ligands through alterations in membrane tension[37], but whether temperature TRPV4

activation is affected remains unknown. As temperature affects lipid order, differences in lipid order between control and ePL-producing S2R+ cells might be an underlying mechanism for the altered temperature threshold of *Drosophila* TRPA1. For example, a previous report claimed that increasing unsaturated FAs in the cell membrane, which should increase lipid disorder, resulted in enhanced heat responsiveness of TRPA1 neurons and decreased preferred temperature of *Drosophila* larvae[19]. Further research is needed to clarify the parameters of cell membrane properties involved in regulating the temperature threshold of TRPA1 activation.

An intriguing question is whether ePLs can directly modulate channel functions through direct binding to specific sites aside from altering membrane properties. Various lipid molecules directly interact with TRP channels to modulate their functions[8], including temperature sensitivity. For example, temperature threshold modification in mammalian TRPM8 is regulated by interaction with PIP_2[45]. Further, TRP channels can possess a phospholipid-binding site in the S4–S5 linker domain, which TRPA1 has[46]. The difference between ePLs and general phospholipids lies in the type of linkage between the hydrocarbon chains at the *sn*-1 position in the glycerol backbone: ether phospholipids have a (vinyl) ether linkage whereas phospholipids have an ester linkage. In case of ester bonds, the oxygen molecule at the α-carbon can form hydrogen bonds and affect intermolecular interactions. Although the interaction at the polar head group of PL has been mainly discussed in TRP channels[47], the differential interaction between ether and ester bond at the *sn*-1 position of PL backbone may also be involved in the formation of lipid-TRP channel interactions. Moreover, our results revealed that ePE, rather than ePC, may be crucial for modulating TRPA1 function by comparing HEK293T cells (Supplementary Fig. 3) and ePL-producing S2R+ cells (Fig. 3, Supplementary Fig. 6). These observations may emphasize the contribution of the direct interaction between TRP channels and membrane phospholipids, especially ePEs, in addition to the modification of membrane properties. For PIEZO, the asymmetric distribution of PS in the lipid bilayer mostly regulates the channel[15]. Moreover, lipid binding was observed in the cryo-electron microscopy structural analysis of PIEZO1 in lipid nanodiscs[44]. Although the structures of PIEZO channels and all the thermosensitive TRP channels including TRPA1 have been solved at an atomic level, how lipid molecules contribute to mechanical or temperature channel activation remains unclear. Future research may clarify the structural and functional coupling of membrane lipids including ePLs and TRP channels.

350 This study demonstrated the expression of the ether lipid synthesis enzyme, AGPS, and
351 the presence of ether lipids in the CNS of *Drosophila*. Product ion scan analysis of major ePL
352 species in the CNS showed a prevalence of plasmanyl-type ePLs, which have no double bond,
353 rather than plasmenyl-types with a vinyl-ether bond. In humans, about 20% of ePLs are
354 plasmenyl-type plasmalogen[21]. The lipidomic analysis of honeybee (*Apis mellifera*) showed
355 abundant non-plasmenyl-type ePLs in the CNS[48], suggesting that plasmanyl-type ePLs may be
356 prevalent in the CNS of insects. To date, most discussions focus on the function of
357 plasmenyl-type plasmalogen ePLs. Particularly, on the high sensitivity of the vinyl–ether linkage
358 with a double bond to reactive oxygen species and its correlation with oxidative stress[49]. In
359 contrast, our study clearly identified the functional roles of nonplasmenyl-type ePLs on sensory
360 channels. While the possibility of a correlation between changes in cell membrane tension due to
361 oxidative stress and the activation of mechanoreceptor channels and cell death have been
362 discussed[50], the changes in cell membrane properties caused by ePLs shown in this study may be
363 another molecular basis for the intrinsic sensory regulation in cells and animals.
364 Recently, Δ1-desaturase, plasmanylethanolamine desaturase 1 (PEDS1, TMEM189),
365 has been identified as the enzyme responsible for inserting a double bond at the *sn*-1 position of
366 ePLs[51, 52]. However, in *Drosophila*, the putative PEDS1 gene, *Kua*, does not show high
367 expression in the CNS according to FlyAtlas RNA-seq analysis[53]. This could explain the
368 minimal presence of plasmenyl-type ePLs in the CNS of *Drosophila* (Supplementary Fig. 2). It
369 would be interesting to more specifically explore the expression pattern and function of Kua in
370 *Drosophila*. In addition to the CNS, ePLs are abundantly present in glial cells in mammals[54].
371 Since the temperature-dependent motility of microglia is modulated by thermosensitive TRPV4[55]
372 and PIEZO1 activity is reportedly essential for the myelination[56], it would be interesting to test
373 whether ePLs are involved in the regulation of these channels in glial cells.
374 In conclusion, we showed that ePLs modulate distinct functions of the sensory proteins
375 such as TRPA1 and PIEZO. Since somatosensory channel proteins are involved in various
376 physiological functions[57, 58], exploring the integrative roles of ePLs as a regulator of receptor
377 proteins may shed light on the various biological processes and diseases related to channel
378 proteins.
379

380 **METHODS**

381 **Fly stocks and husbandry**

382 w^{1118} was used as a control unless otherwise specified. The following strains were obtained from
383 Bloomington Drosophila Stock Center (BL) or Vienna Drosophila RNAi Center (VDRC):
384 5×*UAS-mCD8::GFP* (BL #5137), *piezo-GAL4* (BL #59266), *painless-GAL4* (BL #27894),
385 *UAS-dicer-2* on II (VDRC #60008), *UAS-dicer-2* on III (VDRC #60009), and *UAS-AGPS* RNAi
386 (VDRC #3321). The following stocks were provided by the indicated investigators:
387 *TRPA1-AB*^{GAL4}, *TRPA1-CD*^{GAL4}, *iav-GAL4*, and *TRPL-GAL4* (C. Montell), and *ppk-GAL4* (D. N.
388 Cox). All fly strains were outcrossed to the control line (w^{1118}) for 4–5 generations. Flies were
389 reared on standard cornmeal-yeast medium (19 g agar, 180 g cornmeal, 100 g dry brewer's yeast
390 Ebios, 250 g glucose, 24 mL Methyl 4-hydroxybenzoate [10% w/v solution in 70% ethanol], and
391 8 mL propionic acid in 2500 mL reverse osmosis [RO] water). The flies were reared in a 25°C
392 incubator under a 12-h light/12-h dark cycle.

393

394 **Generation of AGPS knock-out flies**

395 *AGPS* knock-out (*AGPS*^{KO}) flies were generated in our laboratory using the CRISPR-Cas9
396 system. The guide RNA sequence (5′-AATGGCAGCCAAGCGGAATG-3′) was designed using
397 the flyCRISPR target finder (http://targetfinder.flycrispr.neuro.brown.edu/) and cloned into the
398 pU6_3-BbsI-chiRNA vector (Addgene). To achieve homologous recombination, we employed as
399 donor template the pHD-ScarlessDsRed (Drosophila Genomics Resource Center), which
400 contains 1045 bp upstream and 945 bp downstream of the Cas9-mediated double-strand break
401 site in the *AGPS* genome sequence. Subsequently, the constructed vectors were injected into
402 embryos of vas-cas9 on III (BL #51324). Two distinct *AGPS*^{KO} clones, *AGPS*^{KO1} and *AGPS*^{KO2},
403 were obtained and outcrossed individually to the control line (w^{1118}) for five generations. For all
404 experiments, *AGPS*^{KO1} was the designated line unless otherwise specified.

405

406 **Measurement of pupariation time**

407 To enhance egg production, flies were introduced into vials containing standard food
408 supplemented with a yeast paste for ≥48 h following CO_2 exposure. Flies were transferred to new
409 vials containing standard food for egg laying for 3 h. These vials were placed inside a plastic bag
410 with water supply to maintain high humidity before measurements. The number of pupae on the

411 vial wall was counted during the light period, 114–192 h AEL. To determine the time at which
412 50% of the animals underwent pupariation (T_{50}), we utilized the maximum number of pupae
413 observed in each vial and performed linear regression analysis on the growth curve.
414
415 **Quantitative PCR for *Drosophila* larvae and cells**
416 To prepare the whole body sample of late third instar larvae (120 h AEL), 10 larvae were
417 collected and rinsed in RO water twice. To isolate the tissues, the larvae were placed in ice-cold
418 phosphate-buffered saline (PBS), and the body wall cuticles were carefully opened using micro
419 scissors. After removing the guts and major tracheal organs, the CNS (brain and ventral nerve
420 cord), fat body, and carcass (body wall cuticles) were collected. Tissues were obtained from 5–10
421 larvae. Whole body or tissue samples were homogenized by a pestle in Sepasol-RNA I Super G
422 (Nacalai Tesque). For culture cell samples, human embryonic kidney 293T (HEK293T) cells or
423 *Drosophila* S2R+ cells were grown in 60-mm dishes at 37 or 25ºC, respectively, until reaching
424 confluence. Then, cells were washed with PBS and homogenized in Sepasol-RNA I Super G
425 (Nacalai Tesque). Total RNA was extracted following the manufacturer's protocol.
426 To isolate *ppk*-positive peripheral sensory neurons from late third instar larvae
427 expressing mCD8 in *ppk-GAL4* neurons (*UAS-mCD8::GFP*; *ppk-GAL4*), magnetic-bead-based
428 cell sorting was utilized as previously reported[59], with modifications. Fifty larvae were placed in
429 ice-cold PBS, and the posterior end was excised. The cuticle was inverted, and the internal
430 organs removed. Cuticles were then transferred into a microtube and treated with 50 µg/µL
431 Liberase and 20 mU/µL DNase in 1 mL PBS supplemented with 0.02% Tween 20 (PBSTw) for
432 30 min at 25ºC with agitation. The homogenates were filtrated through a 100 µm mesh and
433 further filtrated through a 30 µm mesh to remove debris. All apparatuses were coated with 0.1%
434 globulin free-bovine serum albumin (BSA; 016-15111, Wako). Dissociated cells were then
435 collected by centrifugation for 20 min at 300 ×*g*, and the supernatant was removed. Next, cells
436 were resuspended in PBSTw and precleared with protein G Dynabeads for 10 min at 4ºC with
437 rotation. The cell suspension was then incubated with α-CD8 antibody-coated protein G
438 Dynabeads for 20 min at 4ºC with rotation. Bead-attached cells were collected using a magnetic
439 stand and washed with PBS five times. Total RNA was extracted from bead-bound cells using
440 NucleoSpin RNA Plus XS (Macherey–Nagel) following the manufacturer's protocol. The RNA
441 concentration was measured using the QuantiFluor RNA System (Promega).

442 After obtaining the total RNA, cDNA was synthesized using ReverTra Ace. The
443 expression level of the *AGPS* gene was quantified by the ΔΔCt method, using *rp49* as a reference
444 gene; KOD SYBR was used for the qPCR, which was performed on StepOne (Applied
445 Biosystems).
446
447 **Lipid analysis**
448 For *Drosophila* tissues (10 whole bodies and the CNS of late third instar larvae), lipid extraction
449 was performed using the Bligh and Dyer method[60]. Samples were homogenized in MilliQ water
450 on ice and total lipids extracted using a solvent mixture containing water/methanol/chloroform
451 (1:1:1, v/v) twice. For culture cells, total lipids were extracted using the MTBE method[61]. Cells
452 on dish were detached with PBS and collected in a microtube by centrifugation (1000x *g*, 5 min).
453 Then, cells were resuspended in 100 μL MilliQ water, and total lipids extracted using
454 MTBE/methanol/water (10:3:2.5, v/v) twice.
455 The solvent was evaporated under nitrogen gas, and the final total lipid extract
456 redissolved in methanol. Phospholipids, including ether-type phospholipids, were analyzed by
457 LC-MS/MS using LC-30AD coupled to a triple quadrupole mass spectrometer LCMS-8040
458 (Shimadzu), as previously described[19]. For multiple reaction monitoring (MRM), the transition
459 of $[M + H]^+ \rightarrow 184.0$ was used for PC and $[M + H]^+ \rightarrow [M + H]^+ - 141.1$ was used for PE. For the
460 product ion scan analysis of ePEs, $[M–H]^–$ ions were used as precursor ions derived from PE and
461 scan from m/z:350 to m/z:150.
462
463 **Temperature gradient assay**
464 The temperature gradient assay was conducted following the previously described method[62] with
465 modifications. Aluminum trays [180 mm (W) × 40 mm (D) × 5 mm (H)] were coated with 20 mL
466 of 2% agarose. The left and right ends of the tray were placed on top of two aluminum blocks
467 individually temperature-controlled using a circulating water bath. The surface temperature of
468 the agarose was monitored with a thermometer to create a thermal gradient ranging from 8 to
469 35ºC (1.5ºC/cm).
470 Late third instar larvae (120 h AEL) were prepared in the same manner as for
471 pupariation measurements. Larvae were collected and washed twice with an 18% sucrose
472 solution and thoroughly rinsed with RO water twice. After a 10-min recovery period, 30–50

473 larvae were released onto three agarose trays in regions where the surface temperature was
474 approximately 28ºC. Each tray was covered with a clear acrylic lid during the assay. The larvae
475 were allowed to explore the agarose under red LED light (>600 nm) in a black acrylic box. After
476 10 min, the distribution of larvae on the agarose was captured using a digital camera. To quantify
477 the temperature distribution of larvae, the temperature at which each larva was positioned was
478 calculated using the following equation: Temperature (ºC) = Distance from the position at 8ºC
479 (cm) × 1.5 (ºC/cm) + 8ºC. Larvae located within 0.5 cm from the walls or outside the tray were
480 omitted from calculations.
481
482 **Thermal two-way choice assay**
483 The assay was conducted on an aluminum tray [90 mm (W) × 130 mm (D) × 8 mm (H)] coated
484 with 25 mL of 2% agarose. The test tray was placed on top of two adjacent aluminum blocks,
485 separated using a thin plastic film (~1 mm) as spacer. Each block was individually
486 temperature-controlled using a circulating water bath. To prevent agarose from drying, the
487 surface was gently scratched and sprayed with water. The surface temperature on each side of the
488 test tray was confirmed using a thermometer.
489 At the beginning, 40–60 larvae were released at the border between the two
490 temperature zones and allowed to explore the tray under red LED light in a black acrylic box.
491 After 15 min, the distribution of larvae on the tray was captured using a digital camera, and the
492 number of larvae in each temperature zone tabulated. The avoidance index was calculated using
493 the following formula: (Number of larvae on 20ºC − Number of larvae on 29ºC)/Total number of
494 larvae on both sides of the test tray. Larvae within the release zone (1 cm wide) were not counted
495 in either temperature zones and those outside the trays were not included in the calculation.
496
497 **Tactile response assays**
498 Late third instar larvae were prepared as for the temperature gradient assay. The gentle-touch
499 assay was performed as described previously[63]. The anterior end of freely moving larvae was
500 lightly touched with a *Φ* 0.1mm nickel–titanium filament. Larval responses were scored as
501 follows: 0, no response; 1, hesitation; 2, turn or withdrawal of the anterior segments; 3, single
502 reverse contraction; or 4, multiple reverse contraction.

503 For the mechanical nociception assay, von Frey filaments with different forces were
504 fabricated using a nickel–titanium filament[64]. Filament forces were calibrated by measuring the
505 weight required to bend them and converting the values to force using the following equation:
506 force (mN) = weight (g) × gravity acceleration (9.8 m/s²). Larvae were released on a 60 mm dish
507 under a dissection microscope and stimulated once on the center of their body with a filament per
508 larva. The number of larvae responding to the stimuli within 5 s was recorded.
509

510 **Immunohistochemistry**

511 The CNS of late third instar larvae was dissected in a buffer containing 5 mM TES, 10 mM
512 HEPES, 120 mM NaCl, 3 mM KCl, 4 mM $MgCl_2$, 2 mM $CaCl_2$, 10 mM $NaHCO_3$, 10 mM
513 trehalose, 10 mM glucose, and 10 mM sucrose (pH 7.25). The dissected CNS was then placed on
514 12mm ϕ cover glass (C012001, Matsunami) coated with poly-L-lysine and fixed with 4%
515 paraformaldehyde and 0.4% Triton-X100 for 30 min at room temperature. Subsequently, samples
516 were washed with PBS containing 0.3% Triton X100 (PBSTx) and blocked with 5% normal goat
517 serum (NGS) in PBSTx for 30 min at room temperature. Then, samples were incubated with an
518 α-GFP primary antibody (1:500; #A6455, Invitrogen) in 5% NGS/PBSTx overnight at 4ºC,
519 followed by washing with PBSTx. Next, samples were incubated with the secondary antibody
520 (α-Rabbit IgG-Alexa488, 1:1000; #A11034, Invitrogen) in PBSTx for 3 h at 4ºC and washed
521 with PBSTx. Finally, samples were mounted on a glass slide using Fluoromount (Diagnostic
522 BioSystems). Fluorescence was captured using an Olympus FV1200 IX83 confocal microscope
523 equipped with a 30×/1.05 objective lens.
524

525 **HEK293T cell culture, transfection, and generation of *AGPS* KO cells**

526 Cells were cultured in Dulbecco's modified Eagle Medium supplemented with 10% fetal bovine
527 serum (#10437-028, Gibco), 1× GlutaMAX, and 50 mg/mL penicillin/50 units/mL streptomycin
528 at 37ºC in 5% CO_2.

529 The CRISPR-Cas9 system[65] was employed to establish *AGPS* KO HEK293T cells. The
530 guide RNA sequence (5′-CAATTTGACAGCTCATGTAG-3′) was designed using CRISPick
531 (https://portals.broadinstitute.org/gppx/crispick/public) and cloned into the pSpCas9
532 (BB)-2APuro (PX459) vector (Addgene). The plasmid was transfected into cells using
533 lipofectamine 2000 and Plus reagent (Invitrogen) and incubated for 6 h at 37ºC. After changing

534 to standard medium, cells were incubated for 2 days, followed by treatment with 10 μg/mL
535 puromycin. Puromycin-resistant colonies were collected, and successful genome editing was
536 confirmed in each colony using the T7-endonucrease assay[65]. Cells from positive colonies were
537 isolated as individual clones by limiting dilution in a 96-well plate (0.5 cell/well).
538 Nonhomologous end joining at the designated region in the clones was confirmed by genome
539 sequencing. *AGPS* KO cells were maintained with standard medium, supplemented with 10
540 μg/mL puromycin.
541 For the functional dTRPA1-A assay, 1 μg dTRPA1-A in pcDNA3.1(+) vector and 0.1
542 μg pCMV-DsRed vector were co-transfected into control or *AGPS* KO cells (2×10^5 cells in a
543 35-mm dish) using lipofectamine 2000 reagent and Plus reagent (Invitrogen) dissolved in 1X
544 OPTI-MEM I medium, following the manufacturer's protocol. After incubating 3–4 h in a 37ºC
545 incubator, the cells were reseeded on 12-mm cover slips (Matsunami) in a 60-mm dish and
546 further incubated overnight at 33ºC in 5% CO_2.
547
548 **S2R+ cell culture, transfection, and generation of stable cell lines**
549 Cells were cultured in Schneider's *Drosophila* medium (Gibco) supplemented with 10% fetal
550 bovine serum (#10437-028, Gibco), and 50 mg/mL penicillin/50 units/mL streptomycin at 25ºC.
551 For the lipid supplementation experiment, 1 mM lipids were mixed and sonicated in 10
552 mg/mL fatty-acid free BSA/0.9% NaCl solution for 15 min to form a complex. As negative
553 control, the same volume of solvent (ethanol) was mixed with a BSA/NaCl solution. The
554 lipid-BSA complex was diluted in the culture medium to achieve a final concentration of 100 μM
555 lipids and incubated with the cells for 24 h. The following lipids were purchased:
556 1-O-Hexadecyl-rac-glycerol (16-AG; #sc-205917, Santa Cruz), Glycerol 1-Oleyl Ether (18-AG;
557 #G598710, Tront Research chemicals), and 1-Octadecanol (18-OH; #O0006, Tokyo Chemical
558 Industry).
559 For the functional assay of dTRPA1-A and dTRPA1-B, we established stable cell lines
560 expressing each isoform. dTRPA1-A or dTRPA1-B in pMT vectors were co-transfected with
561 pBS-puro using X-tremeGENE 9 DNA transfection reagent (Roche), and stable cells were
562 selected and maintained in the presence of 10 μg/mL puromycin. Metallothionein
563 promoter-dependent dTRPA1 expression was induced by supplementing cells with 500 μM
564 $CuSO_4$ for 24 h. For the functional assay of dTRPA1-A in dAGPS-expressing cells, a cloned cell

565 line stably expressing dAGPS was established. The dAGPS in the pAc5.1-V5-His vector was
566 co-transfected with pBS-puro using the X-tremeGENE 9 DNA transfection reagent. Cells
567 expressing N-term-V5-His-dAGPS were selected in the presence of 10 μg/mL puromycin, and a
568 monoclonal cell line was established using limiting dilution in a 96-well plate (0.5 cell/well).
569 pAc5.1-dTRPA1-A and pAc5.1-EGFP were transiently co-transfected into control or dAGPS
570 stable cells using TransFectin Lipid Reagent (BioRad). After a 24 h incubation, transfection
571 medium was removed and replaced by growth medium, and incubated for another 24 h at 25ºC
572 For the functional assay of dPIEZO, pAc5.1-dPIEZO and pAc5.1-DsRed were transiently
573 co-transfected into control cells using TransFectin Lipid Reagent, as described above.
574
575 **Electrophysiology**
576 For whole-cell patch-clamp recordings, the extracellular bath solution contained 140 mM NaCl,
577 5 mM KCl, 2 mM $MgCl_2$, 2 mM $CaCl_2$, 10 mM HEPES, and 10 mM glucose (pH 7.4 for
578 HEK293T cells and pH 7.2 for S2R+ cells, adjusted with NaOH). The pipette solution for
579 HEK293T cells contained 140 mM KCl, 5 mM EGTA, and 10 mM HEPES (pH 7.4, adjusted
580 with KOH). The pipette solution for S2R+ cells contained 140 mM Cs-Aspartate, 2 mM $MgCl_2$,
581 0.01 mM $CaCl_2$, 1 mM EGTA, and 10 mM HEPES (pH 7.2, adjusted with CsOH). Voltage-clamp
582 recordings were used as described previously[66], with an Axon 200B (Molecular Devices)
583 amplifier and pCLAMP software (version 10.7; Axon Instruments). The membrane potential was
584 held at −60 mV, and experiments were performed at 25ºC. For heat stimulation of TRPA1, the
585 temperature of the bath solution was initially decreased by perfusing a precooled solution (10ºC),
586 then increased by perfusing a prewarmed solution (65ºC). The temperature of the solution near
587 the recorded cell was monitored using a TA-29 thermistor (Warner instrument).
588 The temperature threshold for dTRPA1 activation was determined in Arrhenius plots of
589 whole-cell voltage-clamp recordings using Origin software (OriginLab), as previously
590 described[66]. Log scales of currents were plotted against the reciprocal of the absolute temperature
591 (T). The crossing point of the two fitted lines at which the slope changed in Arrhenius plots was
592 defined as the temperature threshold.
593
594 **Calcium imaging**

595 Cells transiently expressing dPIEZO were loaded with 5 μM Fura 2-AM (Dojindo), 0.02%
596 Pluronic F127, and 500 μM probenecid by incubation in standard culture medium for 60 min at
597 25ºC. The same bath solution for electrophysiological experiments was used for measurements.
598 Fura-2 in cells was excited at 340 and 380 nm, and the emission at 510 nm was monitored with a
599 sCMOS camera (Zyla 4.2 Plus, Andor Technology). Time-lapse images were recorded every 3 s.
600 To activate dPIEZO, 10 μM Yoda1 (TOCRIS) was applied by perfusion. The perfusion flow rate
601 was set at 4 mL/min. Ionomycin (5 μM) was applied at the end of the protocol to calibrate the
602 maximum capacity of Ca^{2+} intake. Data were measured and analyzed using the iQ2 software
603 (Andor Technology), and the ratio (340/380) was calculated with Fiji software[67].
604
605 **Force curve measurement using high-speed AFM**
606 S2R+ cells, with/without 24-h supplementation with 100 μM 18-AG, were used for analysis. The
607 cells were attached on concanavalin A (Nacalai)-coated cover glass for 30 min at room
608 temperature immediately before the experiment. The force curve measurement was performed in
609 the same bath solution used for electrophysiological experiments but supplemented with 0.01%
610 BSA. The AFM used was a tip-scan high-speed AFM (TS-HS-AFM) combined with an optical
611 microscope[68]. Optical images were used to confirm cell position and the positions of stiffness
612 measurements. The cantilevers used were Olympus AC10 cantilevers (length 9 μm, width 2 μm,
613 height 0.13 μm), with a carbon tip grown by electron beam deposition (EBD) at its very end. For
614 these measurements, long EBD tips were used, as they are reportedly beneficial for cell
615 measurements[69]. Using the thermal sweep method[70], the cantilevers' spring constants were
616 determined as 0.093 ± 0.038 Nm^{-1}, their resonance frequency as 433 ± 55 kHz, and their
617 Q-factor as 1.34 ± 0.09 (averages and standard deviations of 6 cantilevers). Before measuring the
618 cells, the cantilever's sensitivity was determined by performing a force map of 50 × 50 curves on
619 a glass substrate and calculating determining the slope of the force curves by a linear fit. The
620 resulting 2500 slopes were then plotted as a histogram and fitted with a Gaussian. The sensitivity
621 was designated as the location of the Gaussian's maximum. For all measurements, the scan size
622 was 1 μm × 1 μm, and the pixel resolution set to either 150 × 150 or 200 × 200 pixels.
623 To measure the mechanical properties of S2R+ cells, the edge of a cell was first located
624 in standard tapping mode with a frame time of 5–10 s. After the cell edge was reached, force
625 curves were recorded with a grid of 50 × 50 curves in between topography lines. This force

626 mapping procedure was based on inline force curve measurements[71]. Simultaneously, optical
627 microscopy images were acquired to assign each force map to a cell position. The frame time
628 during force mapping was 30–35 s. Force curves were recorded with a frequency of 1 kHz. The
629 maximum force was not controlled but was typically <500 pN. Only the flat outer regions of
630 cells were measured because the region close to the nucleus exhibited a steep upward slope that
631 prevented stable scanning conditions. Similarly, it was not possible to scan stably directly on top
632 of the nucleus due to part of the cells fluctuating and being deformed by the small lateral
633 scanning forces.
634 The acquired force curves were fitted with the Hertz contact mechanics model
635 assuming a tip radius of 5 nm. Force curves were automatically analyzed using home-made
636 software based on IgorPro. Before fitting the force curve with the Hertz model, the linear
637 background was subtracted from the force curves to level the curves.
638
639 **Imaging-based membrane property measurement**
640 S2R+ cells, with/without 24-h supplementation of 100 μM 18-AG, were used for analysis. Cells
641 were plated on a noncoat glass bottom dish (35mm ϕ, No.1S, D11530H, Matsunami) and
642 incubated for 24 h. Subsequently, the cells on the glass were washed with the same bath solution
643 used for electrophysiological experiments and incubated with either 2 μM Flipper-TR
644 (Spirochrome) or 100 nM LipiORDER (Funakoshi) in the bath solution for 15 min at room
645 temperature. Images were captured using a Leica TCS SP8 FALCON confocal microscope
646 equipped with a HC PL APO CS2 100×/1.40 OIL immersion objective lens, a pulsed
647 supercontinuum white light laser and HyD-SMD photon counting detectors. Images were
648 acquired at 256 × 256 pixels using 3× zoom. For Flipper-TR measurements, we performed
649 excitation at 488 nm and emission at 550–650 nm. The fluorescence lifetimes were calculated
650 from decay curves using Leica LAS X Single Molecule Detection software. The fitting model
651 was an n-exponential reconvolution with instrument response function and two exponential
652 components were estimated. The longer decay time was used for subsequent analysis. For
653 LipiORDER measurement, cells were excited at 405 nm, and the emission spectrum was
654 measured from 450 nm to 650 nm with a 25-nm interval. The red to green ratio (R/G ratio) was
655 calculated by dividing fluorescence intensities at 550–650 nm by those at 450–550 nm. The
656 optical section was set at 80 nm and 50 nm for Flipper-TR and LipiORDER, respectively.

Statistical analysis

Data are presented as means ± SEMs. The times each experiment was performed (n) is indicated either in figure legends or panels. To compare two samples, unpaired, two-tailed Student's *t* tests were performed. To performed multiple comparison, Tukey's test or Dunnett test was used. For comparison of temperature preference behavioral experiment and membrane property assay, nonparametric Mann–Whitney's U-test (for two samples) and Kruskal–Wallis tests followed by Steel's tests (for multiple comparisons vs. control) were performed. All statistical analyses were conducted using Prism 10 (GraphPad) or JMP 14.2 software (SAS Institute). A p-value of less than 0.05 was considered statistically significant.

ACKNOWLEDGMENT

The fly stocks used in this study were obtained from the Bloomington Drosophila Stock Center, and NIG-FLY Stock Center. We thank Dr. Shoma Sato, Naomi Fukuta, Terumi Hashimoto, and Dr. Jing Lei (ExCELLS/NIPS) for supporting fly maintenance and molecular cloning experiments. We appreciate Dr. Masato Umeda (HoloBio Inc.), Dr. Akifumi Shiomi (RIKEN), and Dr. Akira Murakami (University of Shizuoka) for giving us the kind advises to the project.

FUNDING

This work was supported by Grant-in-aid for Scientific research 19K23790 and 21K15192 (for T. Suito), 21H02531 (for T. Sokabe), and 22H04926 (for T.N.) from Japan Society for the Promotion of Science (JSPS) and Ministry of Education, Culture, Sports, Science and Technology, Grant-in-Aid for Transformative Research Areas — Platforms for Advanced Technologies and Research Resources "Advanced Bioimaging Support" JP22H04926 (for T. Sokabe) from JSPS, and the Japan Agency for Medical Research and Development (AMED)-PRIME 23gm6510014h0002 (for T. Sokabe) from AMED.

AUTHORS CONTRIBUTION

T. Suito contributed to designing, conducting and analyzing most of the experiments, preparing the draft and the final version of manuscript. T. Sokabe contributed to supervising the project, preparing the draft and the final version of manuscript. M. Tominaga contributed to supervising

688 the project. K.N. contributed to supervising and performing the LC-MS lipid analysis. X. D.
689 contributed to performing fly behavioral experiments. C.G. and T.U. contributed to supervising
690 and conducting the force curve measurement using AFM. M. Tsutsumi and T.N. contributed to
691 supervising chemical probe-based membrane property measurement. Y.H. contributed to
692 dPIEZO cloning and supervising the calcium measurement experiment.
693
694 **COMPETING INTERESTS**
695 The authors declare that they have no conflicts of interest with the contents of this article.
696

697 **REFERENCES**

698 1. Caterina MJ, Schumacher MA, Tominaga M, Rosen TA, Levine JD, Julius D. The
699 capsaicin receptor: a heat-activated ion channel in the pain pathway. *Nature* **389**, 816-824
700 (1997).
701 2. Dhaka A, Murray AN, Mathur J, Earley TJ, Petrus MJ, Patapoutian A. TRPM8 is required
702 for cold sensation in mice. *Neuron* **54**, 371-378 (2007).
703 3. Moqrich A*, et al.* Impaired thermosensation in mice lacking TRPV3, a heat and camphor
704 sensor in the skin. *Science* **307**, 1468-1472 (2005).
705 4. Coste B*, et al.* Piezo1 and Piezo2 are essential components of distinct mechanically
706 activated cation channels. *Science* **330**, 55-60 (2010).
707 5. Tominaga M*, et al.* The cloned capsaicin receptor integrates multiple pain-producing
708 stimuli. *Neuron* **21**, 531-543 (1998).
709 6. Ranade SS*, et al.* Piezo2 is the major transducer of mechanical forces for touch sensation
710 in mice. *Nature* **516**, 121-125 (2014).
711 7. Kashio M, Tominaga M. TRP channels in thermosensation. *Curr Opin Neurobiol* **75**,
712 102591 (2022).
713 8. Ciardo MG, Ferrer-Montiel A. Lipids as central modulators of sensory TRP channels.
714 *Biochim Biophys Acta Biomembr* **1859**, 1615-1628 (2017).
715 9. Bradshaw HB, Raboune S, Hollis JL. Opportunistic activation of TRP receptors by
716 endogenous lipids: exploiting lipidomics to understand TRP receptor cellular
717 communication. *Life Sci* **92**, 404-409 (2013).
718 10. Sisignano M, Bennett DL, Geisslinger G, Scholich K. TRP-channels as key integrators of
719 lipid pathways in nociceptive neurons. *Prog Lipid Res* **53**, 93-107 (2014).
720 11. Taberner FJ, Fernandez-Ballester G, Fernandez-Carvajal A, Ferrer-Montiel A. TRP
721 channels interaction with lipids and its implications in disease. *Biochim Biophys Acta*
722 **1848**, 1818-1827 (2015).
723 12. Cordero-Morales JF, Vasquez V. How lipids contribute to ion channel function, a fat
724 perspective on direct and indirect interactions. *Curr Opin Struct Biol* **51**, 92-98 (2018).
725 13. Romero LO*, et al.* Dietary fatty acids fine-tune Piezo1 mechanical response. *Nat*
726 *Commun* **10**, 1200 (2019).
727 14. Romero LO*, et al.* Linoleic acid improves PIEZO2 dysfunction in a mouse model of
728 Angelman Syndrome. *Nat Commun* **14**, 1167 (2023).

729 15. Tsuchiya M*, et al.* Cell surface flip-flop of phosphatidylserine is critical for
730 PIEZO1-mediated myotube formation. *Nat Commun* **9**, 2049 (2018).
731 16. Bazinet RP, Laye S. Polyunsaturated fatty acids and their metabolites in brain function
732 and disease. *Nat Rev Neurosci* **15**, 771-785 (2014).
733 17. Custers, Emma EM, Kiliaan, Amanda J. Dietary lipids from body to brain. *Prog Lipid*
734 *Res* **85**, 101144 (2022).
735 18. Vasquez V, Krieg M, Lockhead D, Goodman MB. Phospholipids that contain
736 polyunsaturated fatty acids enhance neuronal cell mechanics and touch sensation. *Cell*
737 *Rep* **6**, 70-80 (2014).
738 19. Suito T, Nagao K, Takeuchi K, Juni N, Hara Y, Umeda M. Functional expression of
739 Delta12 fatty acid desaturase modulates thermoregulatory behaviour in Drosophila. *Sci*
740 *Rep* **10**, 11798 (2020).
741 20. Snyder F. The ether lipid trail: a historical perspective. *Biochim Biophys Acta* **1436**,
742 265-278 (1999).
743 21. Braverman NE, Moser AB. Functions of plasmalogen lipids in health and disease.
744 *Biochim Biophys Acta* **1822**, 1442-1452 (2012).
745 22. de Vet EC, Ijlst L, Oostheim W, Wanders RJ, van den Bosch H.
746 Alkyl-dihydroxyacetonephosphate synthase. Fate in peroxisome biogenesis disorders and
747 identification of the point mutation underlying a single enzyme deficiency. *J Biol Chem*
748 **273**, 10296-10301 (1998).
749 23. Dorninger F, Forss-Petter S, Berger J. From peroxisomal disorders to common
750 neurodegenerative diseases - the role of ether phospholipids in the nervous system. *FEBS*
751 *Lett* **591**, 2761-2788 (2017).
752 24. Razeto A*, et al.* The Crucial Step in Ether Phospholipid Biosynthesis: Structural Basis of
753 a Noncanonical Reaction Associated with a Peroxisomal Disorder. *Structure* **15**, 683-692
754 (2007).
755 25. Im SH, Galko MJ. Pokes, sunburn, and hot sauce: Drosophila as an emerging model for
756 the biology of nociception. *Dev Dyn* **241**, 16-26 (2012).
757 26. Shiomi A*, et al.* Extreme deformability of insect cell membranes is governed by
758 phospholipid scrambling. *Cell Rep* **35**, 109219 (2021).
759 27. Luo J, Shen WL, Montell C. TRPA1 mediates sensation of the rate of temperature change
760 in Drosophila larvae. *Nature neuroscience* **20**, 34-41 (2017).

761 28. Rosenzweig M, Kang K, Garrity PA. Distinct TRP channels are required for warm and
762 cool avoidance in Drosophila melanogaster. *Proc Natl Acad Sci U S A* **105**, 14668-14673
763 (2008).
764 29. Kwon Y, Shen WL, Shim HS, Montell C. Fine thermotactic discrimination between the
765 optimal and slightly cooler temperatures via a TRPV channel in chordotonal neurons. *J*
766 *Neurosci* **30**, 10465-10471 (2010).
767 30. Zhong L*, et al.* Thermosensory and nonthermosensory isoforms of Drosophila
768 melanogaster TRPA1 reveal heat-sensor domains of a thermoTRP Channel. *Cell Rep* **1**,
769 43-55 (2012).
770 31. Gu P*, et al.* Polymodal Nociception in Drosophila Requires Alternative Splicing of TrpA1.
771 *Curr Biol* **29**, 3961-3973 e3966 (2019).
772 32. Kim SE, Coste B, Chadha A, Cook B, Patapoutian A. The role of Drosophila Piezo in
773 mechanical nociception. *Nature* **483**, 209-212 (2012).
774 33. Gong J*, et al.* Shear stress activates nociceptors to drive Drosophila mechanical
775 nociception. *Neuron* **110**, 3727-3742 e3728 (2022).
776 34. Zhong L, Hwang RY, Tracey WD. Pickpocket is a DEG/ENaC protein required for
777 mechanical nociception in Drosophila larvae. *Curr Biol* **20**, 429-434 (2010).
778 35. Tracey WD, Jr., Wilson RI, Laurent G, Benzer S. painless, a Drosophila gene essential for
779 nociception. *Cell* **113**, 261-273 (2003).
780 36. Syeda R*, et al.* Chemical activation of the mechanotransduction channel Piezo1. *Elife* **4**,
781 (2015).
782 37. Caires R*, et al.* Omega-3 Fatty Acids Modulate TRPV4 Function through Plasma
783 Membrane Remodeling. *Cell Rep* **21**, 246-258 (2017).
784 38. Colom A*, et al.* A fluorescent membrane tension probe. *Nat Chem* **10**, 1118-1125 (2018).
785 39. Valanciunaite J*, et al.* Polarity Mapping of Cells and Embryos by Improved Fluorescent
786 Solvatochromic Pyrene Probe. *Anal Chem* **92**, 6512-6520 (2020).
787 40. Astudillo AM, Balboa MA, Balsinde J. Compartmentalized regulation of lipid signaling
788 in oxidative stress and inflammation: Plasmalogens, oxidized lipids and ferroptosis as
789 new paradigms of bioactive lipid research. *Prog Lipid Res* **89**, 101207 (2023).
790 41. Fontaine D*, et al.* Roles of endogenous ether lipids and associated PUFAs in the
791 regulation of ion channels and their relevance for disease. *J Lipid Res* **61**, 840-858
792 (2020).

793 42. Zou Y, *et al.* Plasticity of ether lipids promotes ferroptosis susceptibility and evasion.
794 *Nature* **585**, 603-608 (2020).
795 43. Ford DA, Hale CC. Plasmalogen and anionic phospholipid dependence of the cardiac
796 sarcolemmal sodium-calcium exchanger. *FEBS Lett* **394**, 99-102 (1996).
797 44. Yang X, Lin C, Chen X, Li S, Li X, Xiao B. Structure deformation and curvature sensing
798 of PIEZO1 in lipid membranes. *Nature* **604**, 377-383 (2022).
799 45. Fujita F, Uchida K, Takaishi M, Sokabe T, Tominaga M. Ambient temperature affects the
800 temperature threshold for TRPM8 activation through interaction of phosphatidylinositol
801 4,5-bisphosphate. *J Neurosci* **33**, 6154-6159 (2013).
802 46. Suo Y, *et al.* Structural Insights into Electrophile Irritant Sensing by the Human TRPA1
803 Channel. *Neuron* **105**, 882-894 e885 (2020).
804 47. Poveda JA, *et al.* Lipid modulation of ion channels through specific binding sites.
805 *Biochim Biophys Acta* **1838**, 1560-1567 (2014).
806 48. Morfin N, Fillier TA, Pham TH, Goodwin PH, Thomas RH, Guzman-Novoa E. First
807 insights into the honey bee (Apis mellifera) brain lipidome and its neonicotinoid-induced
808 alterations associated with reduced self-grooming behavior. *J Adv Res* **37**, 75-89 (2022).
809 49. Wynalda KM, Murphy RC. Low-concentration ozone reacts with plasmalogen
810 glycerophosphoethanolamine lipids in lung surfactant. *Chem Res Toxicol* **23**, 108-117
811 (2010).
812 50. Hirata Y, *et al.* Lipid peroxidation increases membrane tension, Piezo1 gating, and cation
813 permeability to execute ferroptosis. *Curr Biol* **33**, 1282-1294 e1285 (2023).
814 51. Gallego-Garcia A, *et al.* A bacterial light response reveals an orphan desaturase for
815 human plasmalogen synthesis. *Science* **366**, 128-132 (2019).
816 52. Werner ER, *et al.* The TMEM189 gene encodes plasmanylethanolamine desaturase which
817 introduces the characteristic vinyl ether double bond into plasmalogens. *Proc Natl Acad*
818 *Sci U S A* **117**, 7792-7798 (2020).
819 53. Chintapalli VR, Wang J, Dow JAT. Using FlyAtlas to identify better Drosophila
820 melanogaster models of human disease. *Nature Genetics* **39**, 715-720 (2007).
821 54. Barnes-Velez JA, Aksoy Yasar FB, Hu J. Myelin lipid metabolism and its role in
822 myelination and myelin maintenance. *Innovation (Camb)* **4**, 100360 (2023).
823 55. Nishimoto R, *et al.* Thermosensitive TRPV4 channels mediate temperature-dependent
824 microglia movement. *Proc Natl Acad Sci U S A* **118**, (2021).

825 56. Acheta J*, et al.* Piezo channels contribute to the regulation of myelination in Schwann
826 cells. *Glia* **70**, 2276-2289 (2022).
827 57. Zhang M, Ma Y, Ye X, Zhang N, Pan L, Wang B. TRP (transient receptor potential) ion
828 channel family: structures, biological functions and therapeutic interventions for diseases.
829 *Signal Transduct Target Ther* **8**, 261 (2023).
830 58. Delmas P, Parpaite T, Coste B. PIEZO channels and newcomers in the mammalian
831 mechanosensitive ion channel family. *Neuron* **110**, 2713-2727 (2022).
832 59. Turner HN*, et al.* The TRP Channels Pkd2, NompC, and Trpm Act in Cold-Sensing
833 Neurons to Mediate Unique Aversive Behaviors to Noxious Cold in Drosophila. *Curr*
834 *Biol* **26**, 3116-3128 (2016).
835 60. Bligh EG, Dyer WJ. A rapid method of total lipid extraction and purification. *Can J*
836 *Biochem Physiol* **37**, 911-917 (1959).
837 61. Matyash V, Liebisch G, Kurzchalia TV, Shevchenko A, Schwudke D. Lipid extraction by
838 methyl-tert-butyl ether for high-throughput lipidomics. *J Lipid Res* **49**, 1137-1146 (2008).
839 62. Sokabe T, Chen HC, Luo J, Montell C. A Switch in Thermal Preference in Drosophila
840 Larvae Depends on Multiple Rhodopsins. *Cell Rep* **17**, 336-344 (2016).
841 63. Kernan M, Cowan D, Zuker C. Genetic dissection of mechanosensory transduction:
842 mechanoreception-defective mutations of Drosophila. *Neuron* **12**, 1195-1206 (1994).
843 64. Lopez-Bellido R, Galko MJ. An Improved Assay and Tools for Measuring Mechanical
844 Nociception in Drosophila Larvae. *J Vis Exp*, (2020).
845 65. Ran FA, Hsu PD, Wright J, Agarwala V, Scott DA, Zhang F. Genome engineering using
846 the CRISPR-Cas9 system. *Nat Protoc* **8**, 2281-2308 (2013).
847 66. Nguyen THD*, et al.* Single amino acids set apparent temperature thresholds for
848 heat-evoked activation of mosquito transient receptor potential channel TRPA1. *J Biol*
849 *Chem* **298**, 102271 (2022).
850 67. Schindelin J*, et al.* Fiji: an open-source platform for biological-image analysis. *Nat*
851 *Methods* **9**, 676-682 (2012).
852 68. Fukuda S*, et al.* High-speed atomic force microscope combined with single-molecule
853 fluorescence microscope. *Rev Sci Instrum* **84**, 073706 (2013).
854 69. Shibata M, Uchihashi T, Ando T, Yasuda R. Long-tip high-speed atomic force
855 microscopy for nanometer-scale imaging in live cells. *Sci Rep* **5**, 8724 (2015).
856 70. Hutter JL, Bechhoefer J. Calibration of atomic-force microscope tips. *Review of Scientific*

857 *Instruments* **64**, 1868-1873 (1993).
858 71. Ganser C, Uchihashi T. Microtubule self-healing and defect creation investigated by
859 in-line force measurements during high-speed atomic force microscopy imaging.
860 *Nanoscale* **11**, 125-135 (2018).
861
862

863 **FIGURE LEGENDS**

864 **Fig. 1 Ether phospholipid enrichment in *Drosophila* neurons.**

865 **a** Relative *AGPS* expression level in different tissues in w^{1118} third instar larvae (n = 3). CNS:
866 central nervous system. *p < 0.05, Tukey's test. **b** Relative *AGPS* expression level in
867 *ppk*-positive peripheral neurons (bead bound) and other cells (bead unbound) (n = 4). ** p < 0.01,
868 Student's t-test. **c** Total ePE area (% of total PE in whole body and the CNS) of third instar larvae
869 (n = 4) in w^{1118} (control), heterozygous *AGPS* knockout ($AGPS^{KO/+}$), and homozygous *AGPS*
870 knockout ($AGPS^{KO/KO}$) are shown. *** p < 0.001, Student's t-test. Each point in **a**–**c** represents a
871 biological replicate. Data are presented as mean ± SEM. **d, e** Colormap for the composition of
872 PE (**d**) and PC (**e**) species (area% of total species) in the CNS of w^{1118} (control) and homozygous
873 $AGPS^{KO}$ third instar larvae (n = 4). Phospholipid molecules are listed as PE (X:Y) or PC (X:Y),
874 where X denotes the total number of carbon molecules in acyl chains and Y the total of double
875 bonds in acyl chains. Cross marks indicate phospholipid species under detectable levels. Source
876 data are provided as a Source Data file.

877

878 **Fig. 2 AGPS regulates TRPA1-A/B-dependent thermosensation.**

879 **a**, **b** Temperature preference assay on a linear gradient for late third instar larvae of w^{1118} (control,
880 n = 16), heterozygous $AGPS^{KO}$ ($AGPS^{KO1/+}$, n = 6), homozygous $AGPS^{KO}$ clones ($AGPS^{KO1/KO1}$
881 and $AGPS^{KO2/KO2}$, n = 9). **c**, **d** Temperature preference assay for late third instar larvae of control
882 (*UAS-AGPS RNAi*/+, n = 13), and *AGPS* knockdown by $TRPA1\text{-}AB^{GAL4}$
883 (*UAS-dicer-2/UAS-AGPS* RNAi;$TRPA1\text{-}AB^{GAL4}$/+, n = 8), $TRPA1\text{-}CD^{GAL4}$ (*dicer-2/AGPS*
884 RNAi;$TRPA1\text{-}CD^{GAL4}$/+, n = 8), *TRPL-GAL4* (*UAS-dicer-2/UAS-AGPS* RNAi;*TRPL-GAL4*/+, n
885 = 8), and *Iav-GAL4* (*UAS-dicer-2/UAS-AGPS* RNAi;*Iav-GAL4*/+, n = 9). **e**, **f** Temperature
886 preference assay for late third instar larvae of control (*UAS-dicer-2/+*;$TRPA1\text{-}AB^{GAL4}$/+, n = 9),
887 *AGPS* knockdown by $TRPA1\text{-}AB^{GAL4}$ (*UAS-dicer-2/UAS-AGPS* RNAi;$TRPA1\text{-}AB^{GAL4}$/+, n = 12),
888 and *TRPA1-AB* knockout ($TRPA1\text{-}AB^{GAL4}/TRPA1\text{-}AB^{GAL4}$, n = 9). Distribution of third instar
889 larvae on a thermal gradient of 8ºC–35ºC (**a, c, e**) and fraction of larvae distributed over 25ºC
890 zones (**b, d, f**). **g, h** Avoidance index on the thermal two-way choice assay at 29 vs. 20ºC of w^{1118}
891 (control, n = 7) and $AGPS^{KO}$ (n = 6) (**g**), or control ($TRPA1\text{-}AB^{GAL4}$/+, n = 6) and *AGPS*
892 knockdown by $TRPA1\text{-}AB^{GAL4}$ (*UAS-dicer-2/UAS-AGPS* RNAi;$TRPA1\text{-}AB^{GAL4}$/+, n = 6) (**h**).
893 Each point represents a biological replicate. Data are presented as mean ± SEM. *p < 0.05; *** p

894 < 0.001 for Mann–Whitney's U-test or Steel's test (vs. control). Source data are provided as a
895 Source Data file.
896
897 **Fig. 3 Establishment of ePL-producing S2R+ cells.**
898 **a** Synthesis pathways of ePLs. Two strategies to increase ePL production in *Drosophila* are
899 shown. (i) Supplementation with 16-AG or 18-AG (1-alkylglycerol) or (ii) *AGPS* overexpression
900 with 18-OH (fatty alcohol) supplementation. FA-CoA, Fatty acyl-CoA; DHAP,
901 dihydroxyacetone phosphate; GNPAT, dihydroxyacetone phosphate acyltransferase; MGAT,
902 monoacylglycerol acyltransferase; CDP, cytidine diphosphate; CPT, choline phosphotransferase;
903 and CEPT, choline/ethanolamine phosphotransferase. **b–e** Lipid composition in control and
904 ePL-producing S2R+ cells (n = 4) for total ePE area% of total PE (**b**), total ePC area% of total
905 PC (**c**), and colormap for composition of PE (**d**) and PC (**e**) species (area% of total PE or PC) in
906 control cells (Control/S2R+), 100 μM 16-AG supplemented cells (16-AG/S2R+),
907 *dAGPS*-expressing cells (Control/S2R+ dAGPS), and 100 μM 18-OH supplemented
908 *dAGPS*-expressing cells (18-OH/S2R+ dAGPS). Phospholipid molecules are listed as PE (X:Y)
909 or PC (X:Y), where X denotes the total number of acyl chains and Y the total of double bonds in
910 acyl chains. Cross marks in (**d, e**) indicate phospholipid species under detectable levels. Each
911 point represents a biological replicate. Data are presented as mean ± SEM. Source data are
912 provided as a Source Data file.
913
914 **Fig. 4 ePLs modulates the temperature threshold for dTRPA1-A activation.**
915 **a–c** Whole-cell patch-clamp recording of dTRPA1 activation with temperature stimulation in
916 dTRPA1 expressing S2R+ cells (**a**), dTRPA1 expressing cells supplemented with 100 μM 16-AG
917 (**b**), and dTRPA1 expressing cells supplemented with 100 μM 18-AG (**c**). Left, representative
918 traces of recordings; right, Arrhenius plots from the traces in the left panels. Temperature
919 thresholds were determined as a crossing point of two fitted lines. **d–g** Quantification of the
920 temperature threshold (**d**) and peak current densities of heat (**e**), 30 μM AITC (**f**), and 300 μM
921 AITC (**g**) stimulation in dTRPA1 expressing cells supplemented with solvent (control), 100 μM
922 16-AG, or 18-AG. Each point represents a biological replicate. The number of replicates (n) is
923 shown in the panels. Data are presented as mean ± SEM. *p < 0.05; Dunnett test (vs. control).
924 Source data are provided as a Source Data file.

925

926 **Fig. 5 AGPS modulates mechanosensory behaviors.**

927 **a** Distribution of scored responses to gentle touch with a nickel–titanium filament in w^{1118}
928 (control) and $AGPS^{KO}$ late third instar larvae (n = 4). 0: no response, 1: hesitation, 2: turn or
929 withdrawal of the anterior segments, 3: single reverse contractile, or 4: multiple reverse
930 contraction. **b** Responses to different forces applied with von Frey filaments (20.1, 47.0, and 70.0
931 mN) in w^{1118} (control, n = 4 or 5) and $AGPS^{KO}$ late third instar larvae (n = 4 or 5). **c** Responses
932 to a von Frey filament (20.1 mN) in control (*UAS-AGPS RNAi*/+, n = 5) and *AGPS* knockdown
933 using *PIEZO-GAL4* (n = 5), $TRPA1\text{-}CD^{GAL4}$ (n = 5), *ppk-GAL4* (n = 5), and *pain-GAL4* (n = 6).
934 Data are presented as mean ± SEM. *p < 0.05, **p < 0.01; student's t-test (**b**) or Dunnett test (vs.
935 control) (**c**). Source data are provided as a Source Data file.

936

937 **Fig. 6 ePLs modify dPIEZO activity in *Drosophila* cells.**

938 **a–c** Representative Fura-2 imaging data for PIEZO in control S2R+ cells and cells supplemented
939 with 100 μM 18-AG. **a** Typical ratiometric images before (Basal, at 60 s) and after 10 μM Yoda1
940 application (Yoda1, at 360 s), and after 5 μM ionomycin application (Ionomycin, at 540 s) in
941 dPIEZO expressing cells (upper) and dPIEZO expressing cells supplemented with 100 μM
942 18-AG (lower). **B, c** Representative calcium level traces in dPIEZO expressing cells (**b**) and
943 18-AG supplemented dPIEZO expressing cells (**c**). **d, e** Proportion of cells responding to Yoda1
944 (Δratio > 2) (**d**) and maximum Δratio response to Yoda1 normalized by the ionomycin response
945 (**e**) in dPIEZO expressing cells (control, n = 10) and 18-AG supplemented dPIEZO expressing
946 cells (18-AG, n = 10). Each point represents a biological replicate; 25—40 cells were analyzed in
947 each assay. Data are presented as mean ± SEM. *p < 0.05, **p < 0.01; Student's t-test. Source
948 data are provided as a Source Data file.

949

950 **Fig. 7 ePLs alters membrane properties of *Drosophila* cells.**

951 **a** Measurement of membrane tension by AFM in S2R+ cells (control) and cells supplemented
952 with 100 μM 18-AG. Data were acquired from 242 different regions of 24 control cells and 213
953 different regions of 27 cells supplemented with 18-AG. The red horizontal lines represent the
954 median and each point the averaged Young's modulus (Pa) of each region. **b** Measurement of
955 membrane tension by FLIM imaging using Flipper-TR in control (n = 45) and 100 μM 18-AG

956 supplemented S2R+ cells (n = 40). The average fluorescent lifetime of each cell is shown as well.
957 Red horizontal lines represent the median and each point a biological replicate. **c** Representative
958 pseudo color images of LipiORDER loaded control (upper) and 100 μM 18-AG supplemented
959 S2R+ cells (lower). Green fluorescence intensity (left, 450—550 nm), red fluorescence intensity
960 (middle, 550—650 nm), and radiometric images of red to green fluorescence intensity (right,
961 R/G ratio). **d** Fluorescence emission spectrum from 450 nm to 650 nm with a 25-nm interval in
962 control (black, n = 46) and 100 μM 18-AG supplemented S2R+ cells (red, n = 45). Data are
963 presented as mean ± SEM. **e** Quantification of red/green fluorescence ratio (R/G ratio). Each
964 value indicates the average R/G ratio of a single cell. Red horizontal lines represent the median
965 and each point a biological replicate. *$p < 0.05$, ***$p < 0.001$; Mann–Whitney U-test. Source
966 data are provided as a Source Data file.

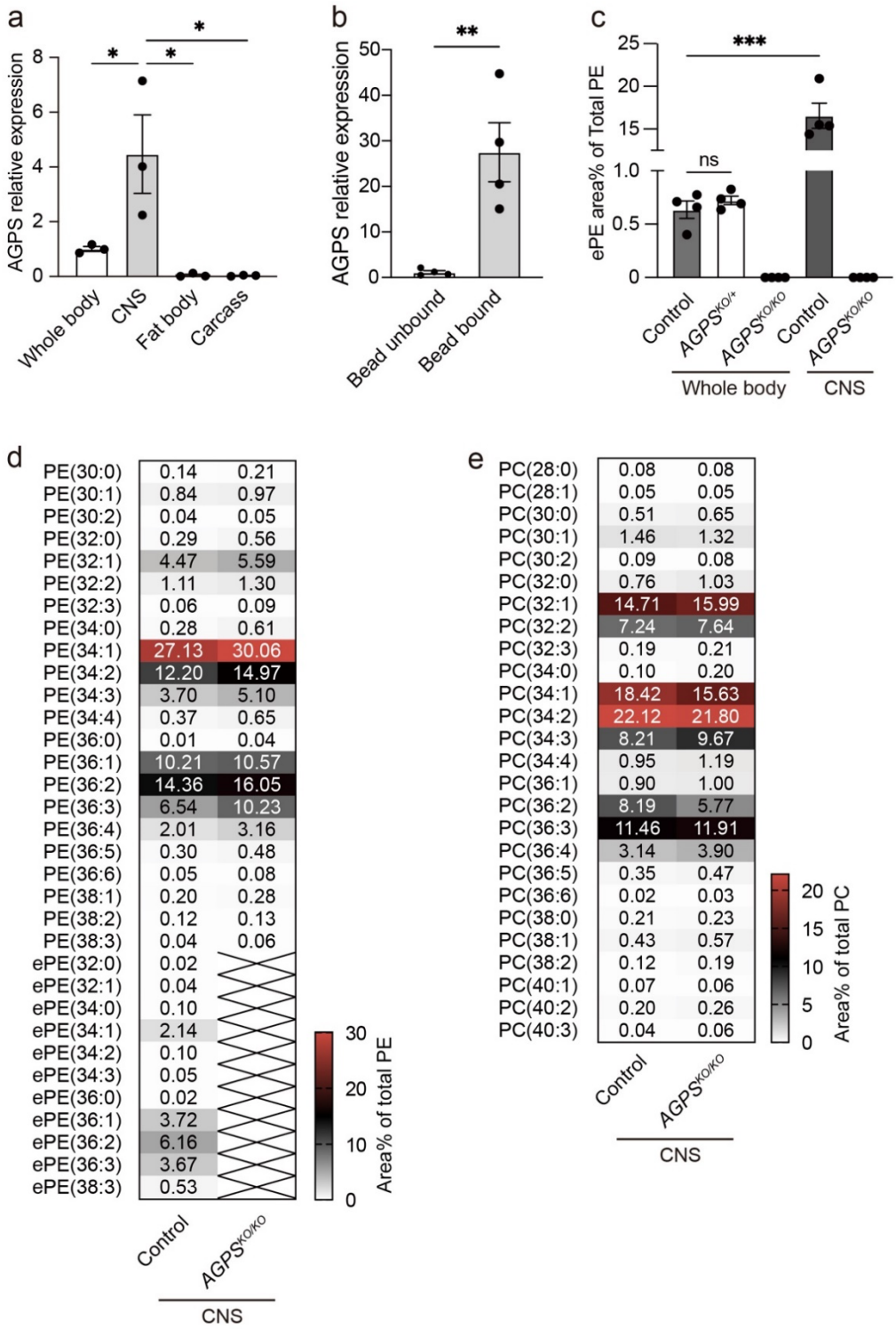

Fig1 Suito et al. 2023

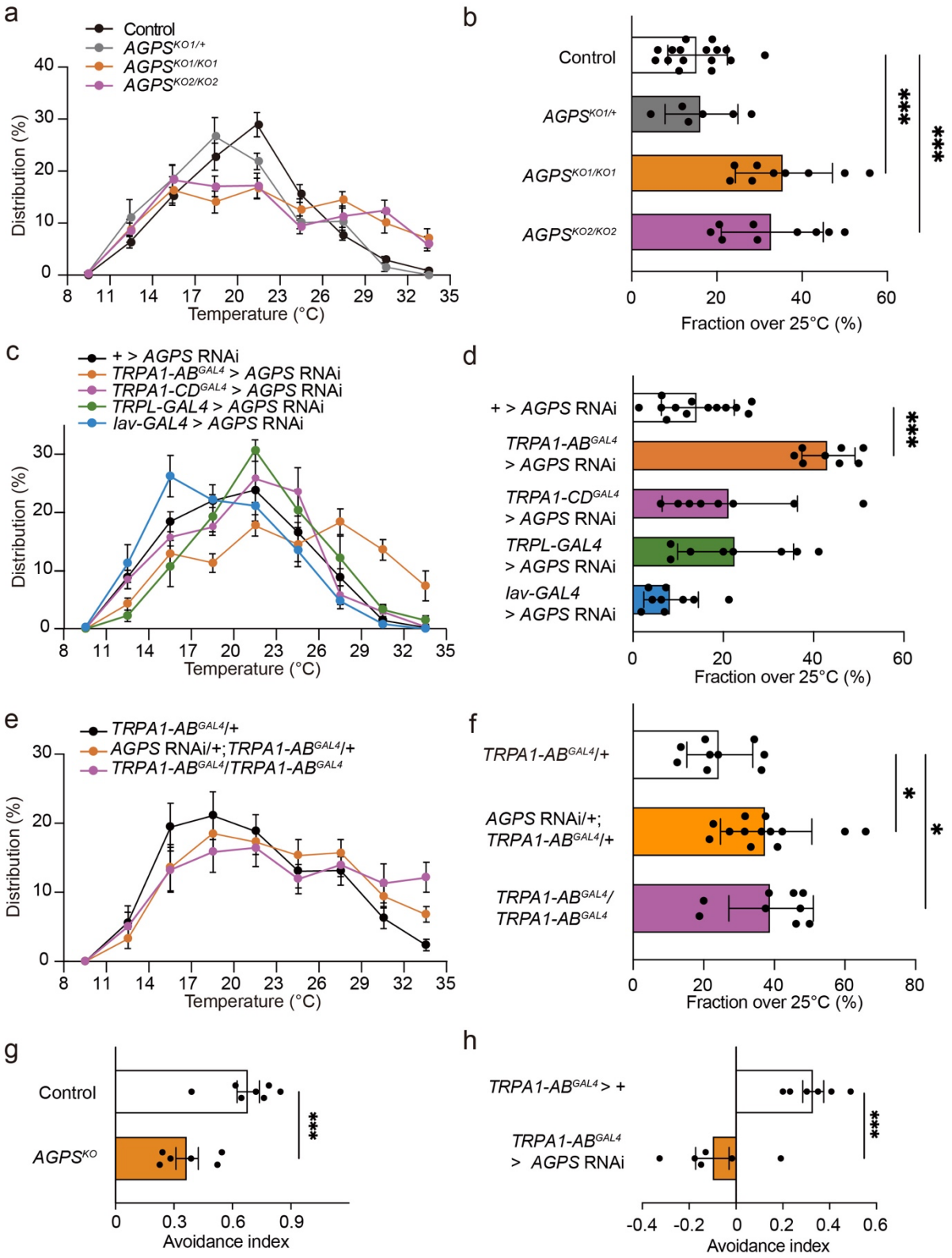

Fig2

Suito et al. 2023

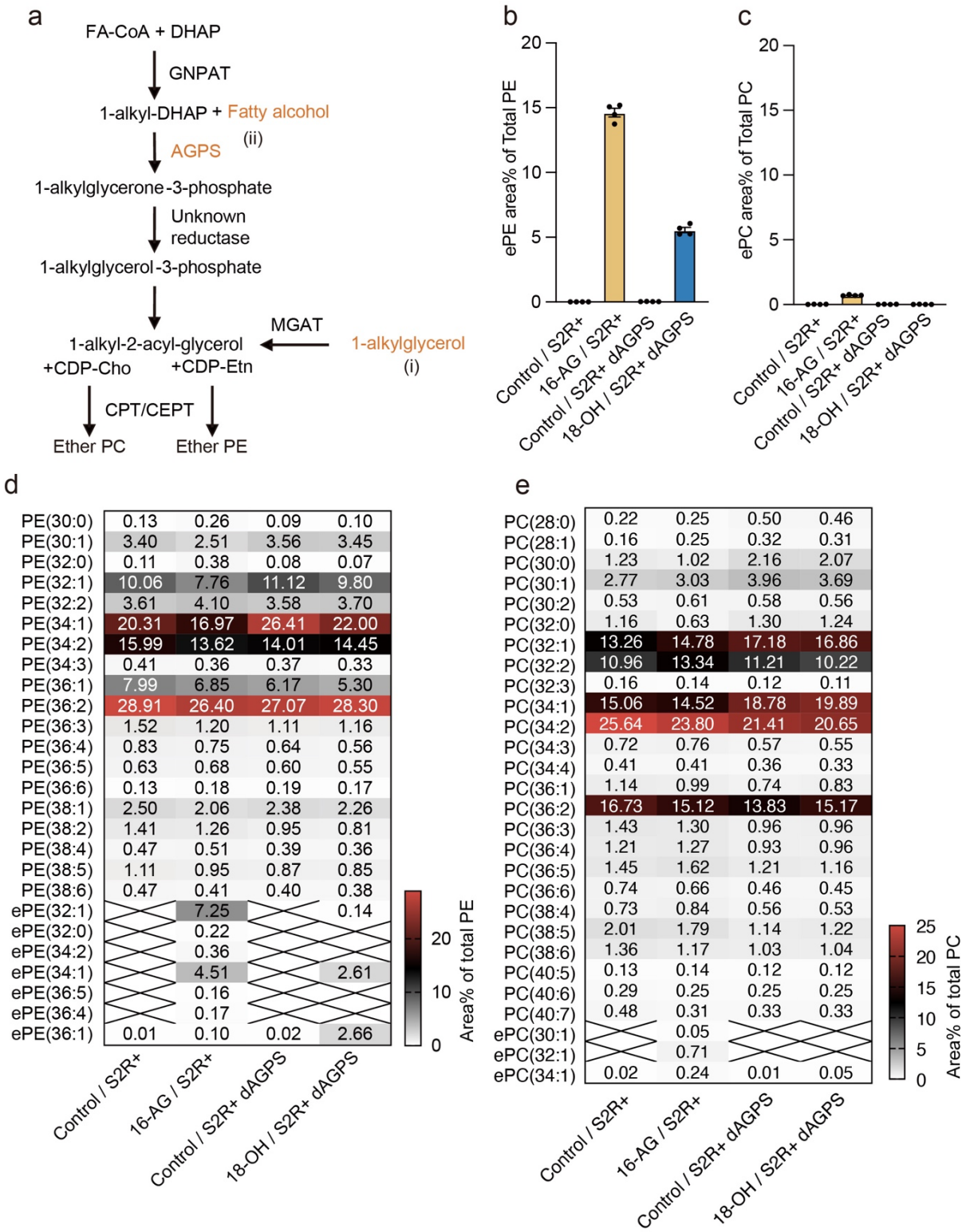

Fig3

Suito et al. 2023

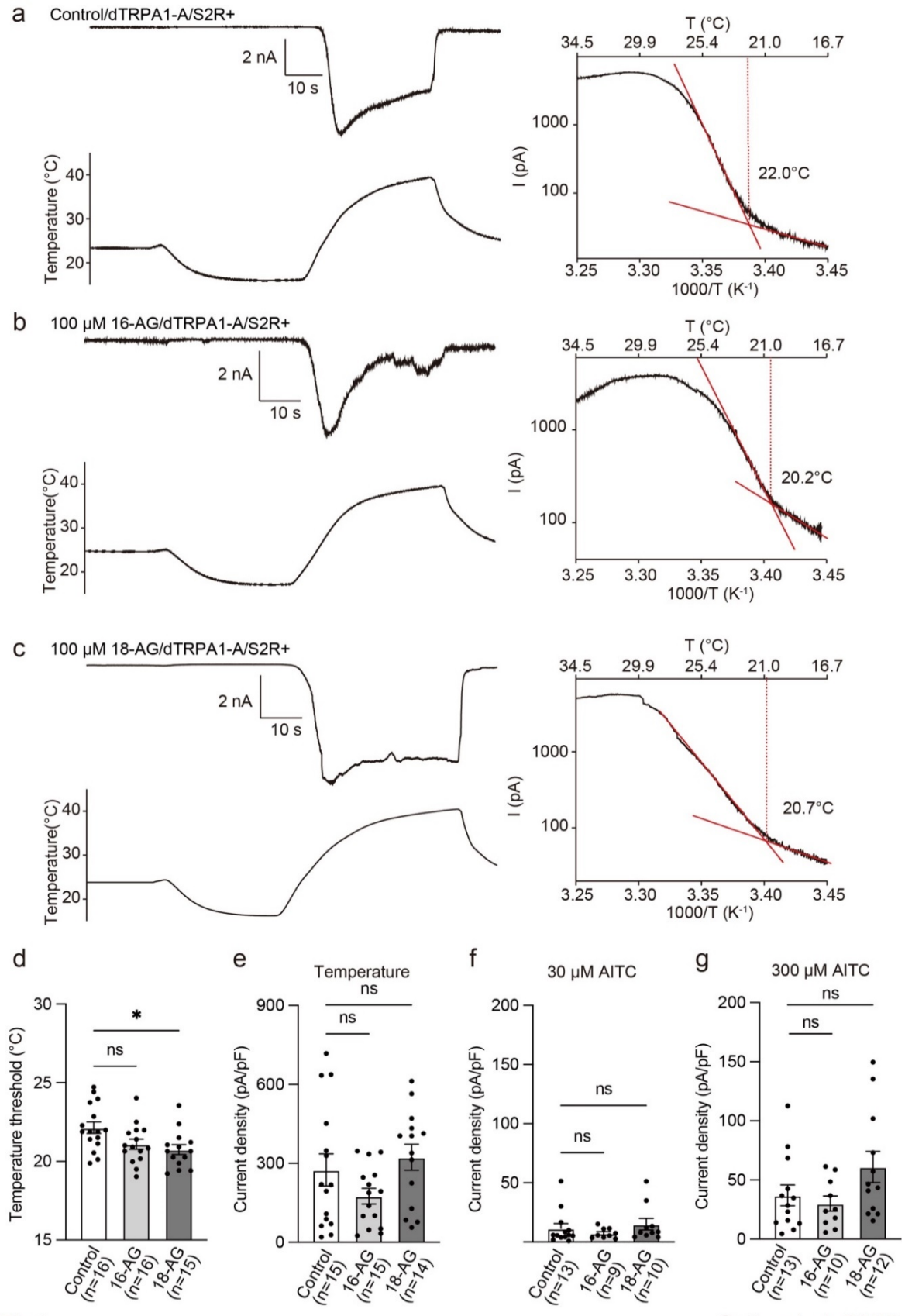

Fig4

Suito et al. 2023

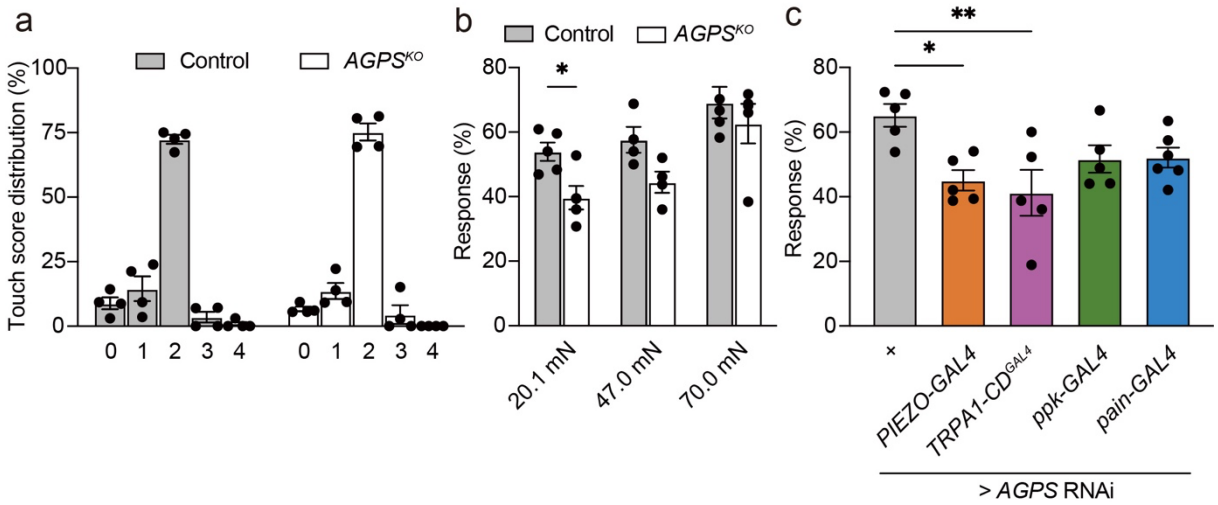

Fig5

Suito et al. 2023

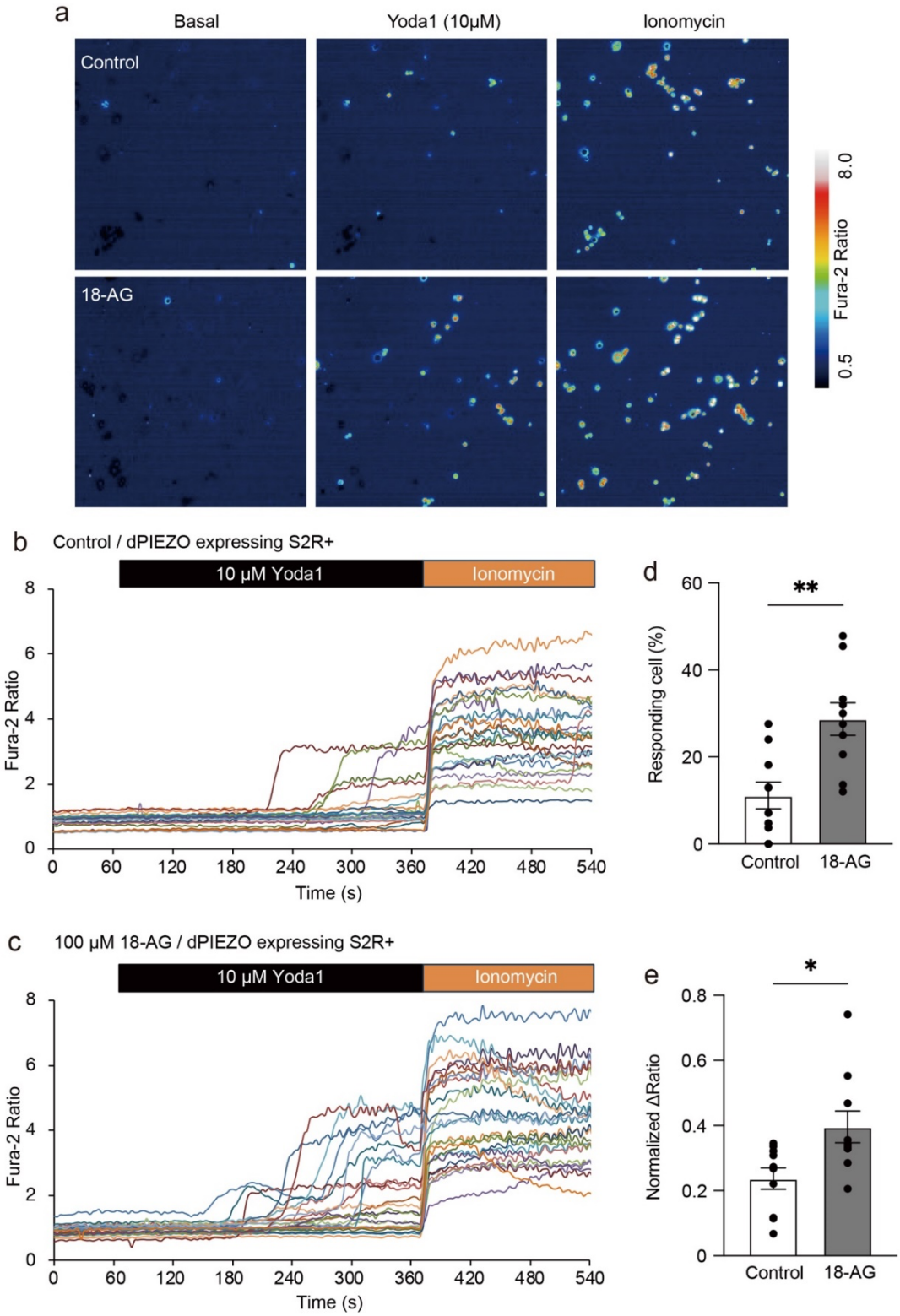

Fig6

Suito et al. 2023

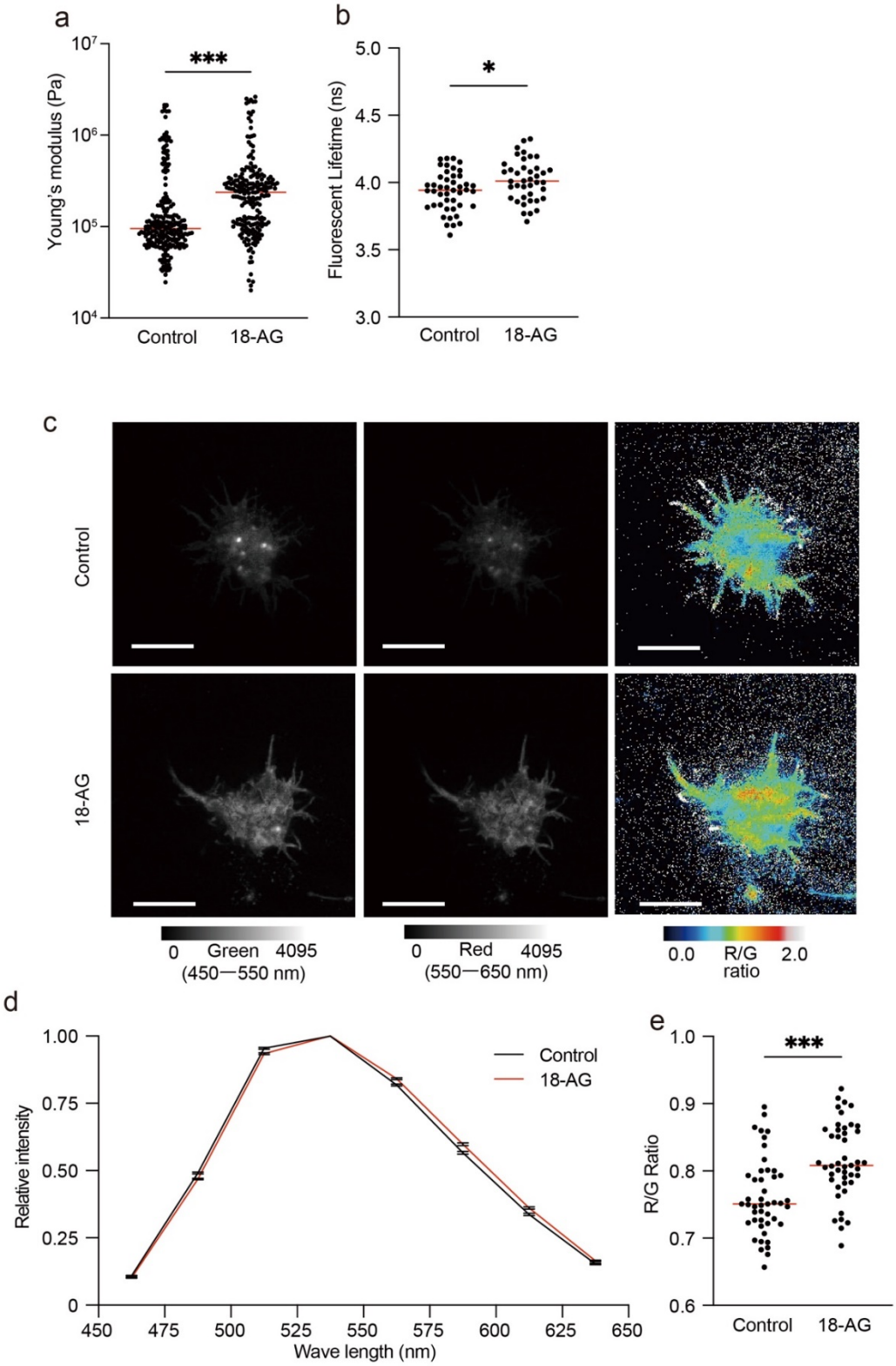

Fig7

Suito et al. 2023